Supporting Information

Table of Contents:

1. General materials and methods

1.1. Materials

The following chemicals were used as received without further purification. Cucurbit[7]uril hydrate (CB7), berberine chloride (BC), phenacetin (≥98.0%), procaine hydrochloride (≥97%), lidocaine hydrochloride monohydrate and levamisole hydrochloride were purchased from Sigma Aldrich. L-ascorbic acid (≥99.0%) was purchased from Fisher Scientific. 1-Adamantanamine ($AdNH_3^+$) hydrochloride (≥99.0%) was purchased from TCI. Analytical drug samples from Cerilliant® were purchased through Sigma Aldrich as 1 mg/mL ampules in methanol or acetonitrile: morphine solution, diazepam solution, etizolam solution, cannabidiol (CBD) solution, Δ^9-tetrahydrocannabinol (Δ^9-THC) solution, (−)-Δ^8- tetrahydrocannabinol (Δ^8-THC) solution, (±)-3,4-methylenedioxymethamphetamine (MDMA) solution, cocaine hydrochloride solution, heroin solution and lorazepam solution.

The DimerDyes DD4, DD8, and DD13 were synthesized and purified following reported protocols.[1] Cucurbit[8]uril (CB8) was synthesized and purified following literature procedures.[2, 3] *N,N'*-dimethyl-2,7-diazapyrenium diiodide (MDAP) was synthesized and purified following the reported protocol.[4]

Street drug samples were collected from Substance, the Vancouver Island Drug Checking Project, located in Victoria, BC, Canada.[5, 6] Solid samples (<10 mg) were submitted by people who use drugs as part of the drug checking service and were analyzed at Substance using established protocols. Fourier transform infrared (FTIR) spectra were collected using a 45° single-bounce attenuated total reflection (ATR) element. The resulting IR spectra were analyzed using classification models for the presence or absence of trace actives.[7] Paper spray-mass spectrometry (PS-MS) analysis was performed to confirm the presence of select target compounds and to provide quantitative concentration information.[8-11] Cases where measurements were above the limit of quantification are reported as >80%, where the lower limit of quantification is approximately 0.1% (weight/weight).[5]

1.2. General UPLC-MS, NMR spectroscopy and MALDI-TOF methods

DimerDye purity was verified using a Waters UPLC-MS equipped with an Acquity UPLC BEH C18 1.7 µm (21 x 50 mm) column, UV/Vis and QDa detector. A gradient of 90% H_2O (0.4% CH_2O_2)/10% CH_3CN (0.4% CH_2O_2) to 30% H_2O (0.4% CH_2O_2)/70% CH_3CN (0.4% CH_2O_2) over 5 minutes at 0.5 mL/min flow was used for all purity traces. All NMR spectra were recorded on a Bruker Avance Neo 500 at 298 K (^{1}H: 500 MHz). ^{1}H NMR performed in phosphate buffer (50 mM, pD 7.4) was prepared using sodium phosphate monobasic and sodium phosphate dibasic in D_2O. The pD was adjusted with 1 M NaOD/DCl and determined using a pH meter.[12]

Mixed host co-assembly of DD13•CB7 was verified by MALDI-TOF MS performed on a Bruker timsTOF *flex* MALDI-2 instrument (Bruker, Breman, Germany) in the positive ion mode. The instrument was calibrated before the experiment in an electrospray mode by a direct infusion of Agilent Calibration mix (Agilent Technologies, Santa Clara, CA, USA). A sample of DD13 (50 µM) and CB7 (50 µM) in NaH_2PO_4/Na_2HPO_4 (2 mM, pH 7.4) in H_2O was deposited (2 uL) onto a steel target plate and then dried under vacuum. A matrix solution of α-cyano-4-hydroxycinnamic acid (CHCA, 12 mg) and ammonium citrate dibasic (3.6 mg) in 30% H_2O/70% CH_3CN+0.1% TFA (4 mL) was prepared. The CHCA matrix solution was deposited (2 uL) on top of the dried sample spot, the plate was then dried again under vacuum.

1.3. General sample preparation for absorbance and fluorescence

Stock solutions of cucurbit[*n*]uril hosts CB7 and CB8 and dyes MDAP and BC were prepared in Milli-Q™ ultrapure water. The concentrations of stock dye solutions MDAP and BC were determined by UV-Vis titration measurements using the reported extinction coefficients (BC, $\varepsilon_{344\ nm}$ = 22300 $M^{-1}cm^{-1}$ and MDAP, $\varepsilon_{393\ nm}$ = 7800 $M^{-1}cm^{-1}$) and Beer-Lambert Law.[13-15] The concentration of cucurbit[*n*]uril stock solutions (CB7 and CB8) was determined in H_2O following reported titration protocols with known strong binding dyes (MDAP and BC, respectively).[13, 14] CB7 was titrated into MDAP, recording the emission at λ_{em} = 454 nm (λ_{ex} = 393 nm). CB8 was titrated into BC, recording the emission at λ_{em} = 542 nm (λ_{ex} = 421 nm). Stock solutions of DimerDyes (1 mM) were prepared by mass in NaH_2PO_4/Na_2HPO_4 (10 mM, pH 7.4) in H_2O. Analytical drug ampules were evaporated overnight under a gentle air stream and redissolved in methanol to form 5.2 mM stock solutions. Solid street drug samples were dissolved in analytical-grade methanol to form 1.5 mg/mL stock solutions.

2. Macrocyclic host synthesis and purity – ^{1}H NMR and UPLC-MS

The calixarene intermediate sCx4-CHO was synthesized following reported protocols.[16] DimerDyes DD4, DD8 and DD13 were synthesized and purified following reported protocols.[1]

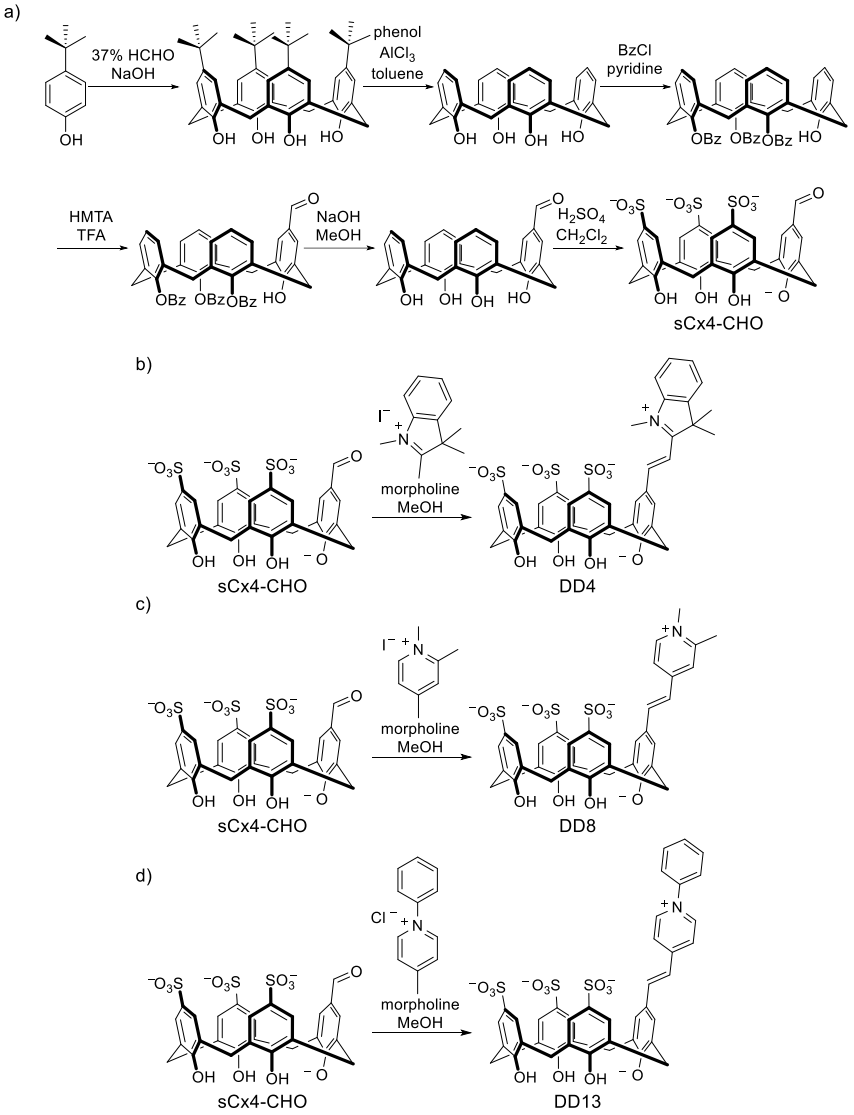

Scheme S1. Synthetic route of a) intermediate sCx4-CHO and synthesis of b) DD4 c) DD8 and d) DD13.[1, 16]

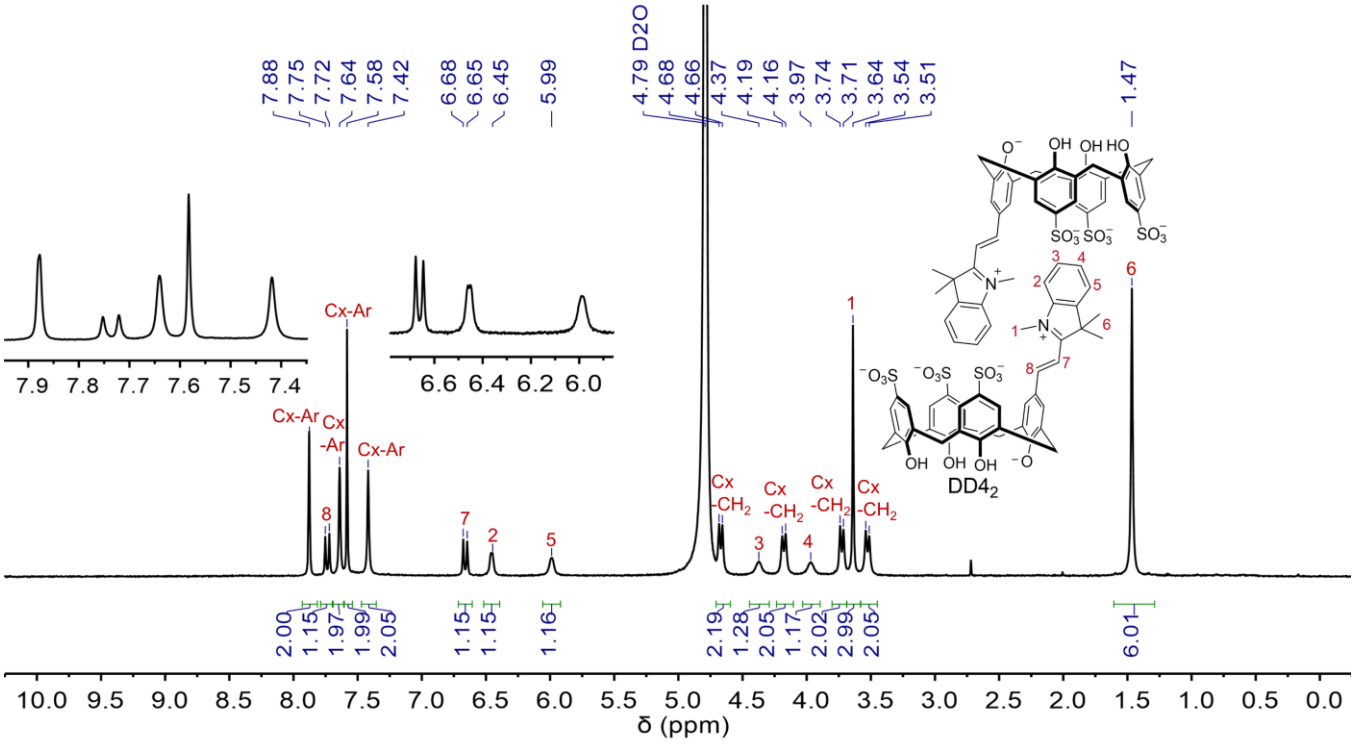

Figure S1. ^{1}H NMR spectrum of $DD4_2$ in NaH_2PO_4/Na_2HPO_4 (50 mM, pD 7.4) in D_2O (500 MHz, 298 K) shows upfield shifted pendant arm methyl and aromatic protons, supporting the existence of the molecule as a homodimer in aqueous solution.

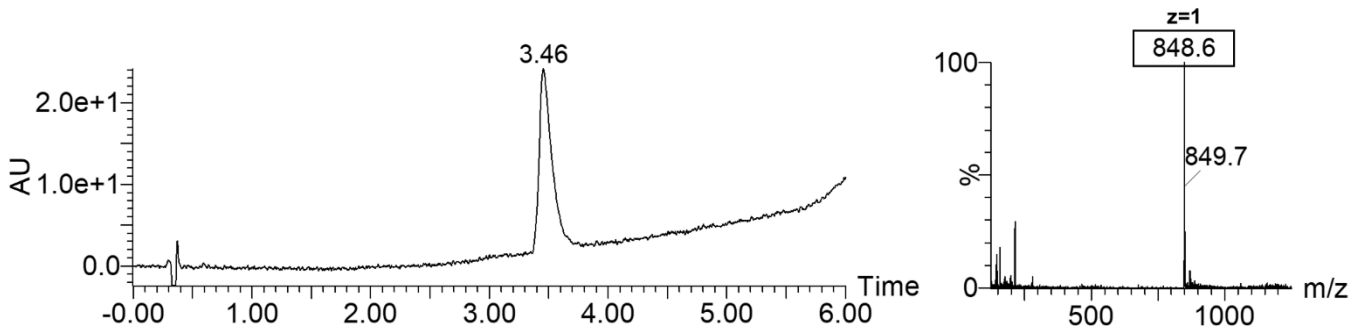

Figure S2. UPLC-MS (ES+) of DD4. Left = UV diode array detected chromatogram (190:400 nm). Right = positive ion mode ESI mass spectrum of the eluted peak.

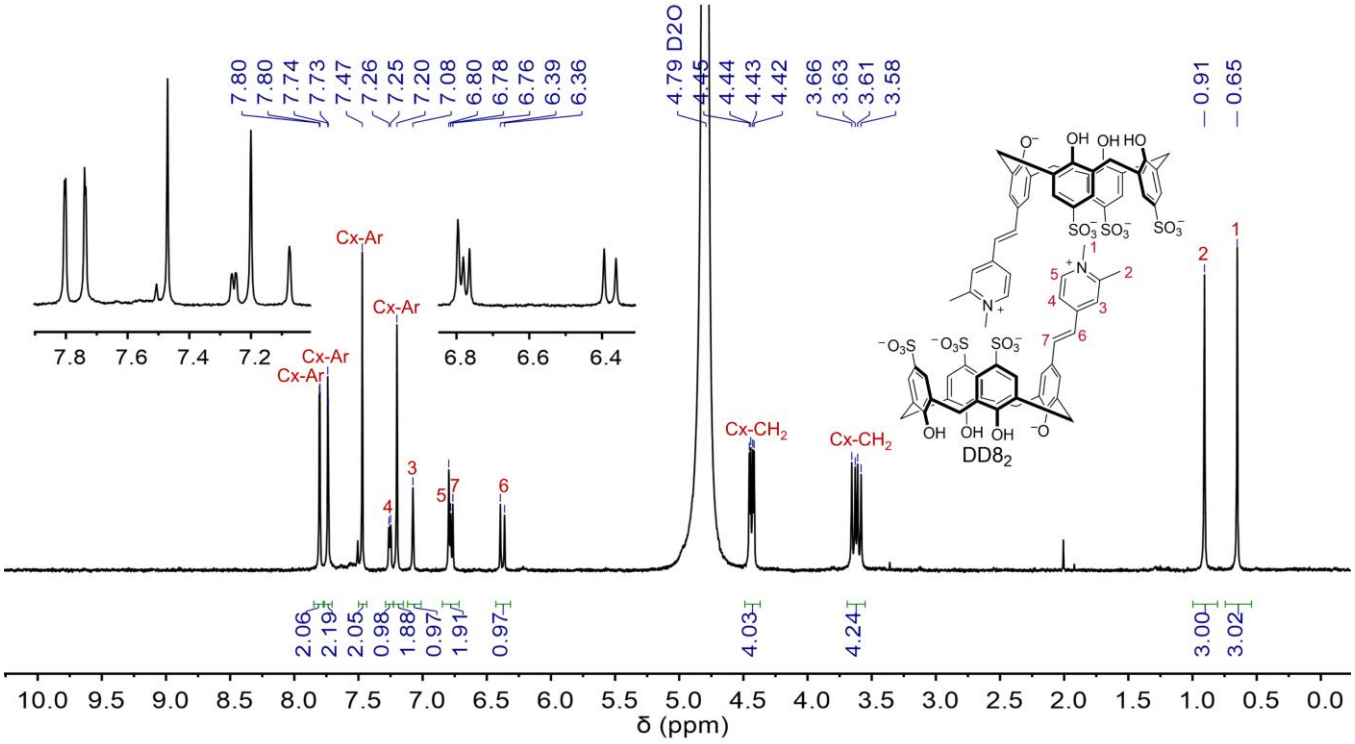

Figure S3. ^{1}H NMR spectrum of DD8$_2$ in NaH_2PO_4/Na_2HPO_4 (50 mM, pD 7.4) in D_2O (500 MHz, 298 K) shows upfield shifted pendant arm methyl and aromatic protons, supporting the existence of the molecule as a homodimer in aqueous solution.

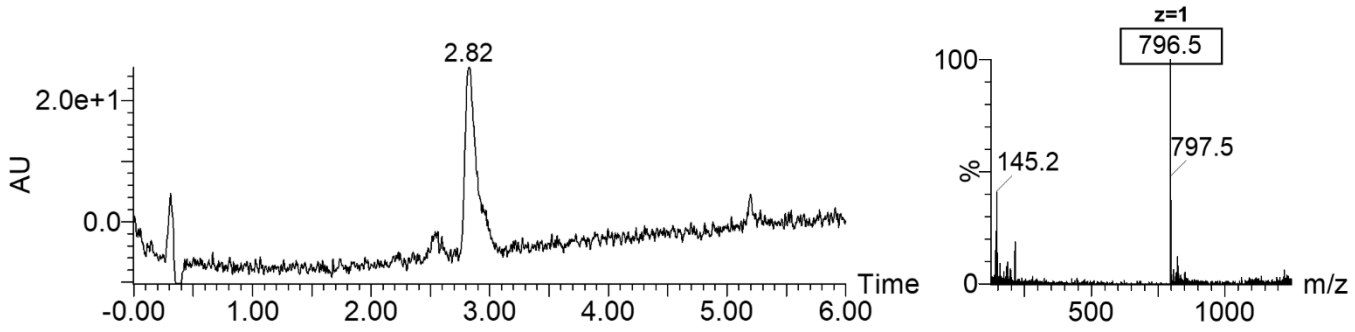

Figure S4. UPLC-MS (ES+) of DD8. Left = UV diode array detected chromatogram (190:800 nm). Right = positive ion mode ESI mass spectrum of the eluted peak.

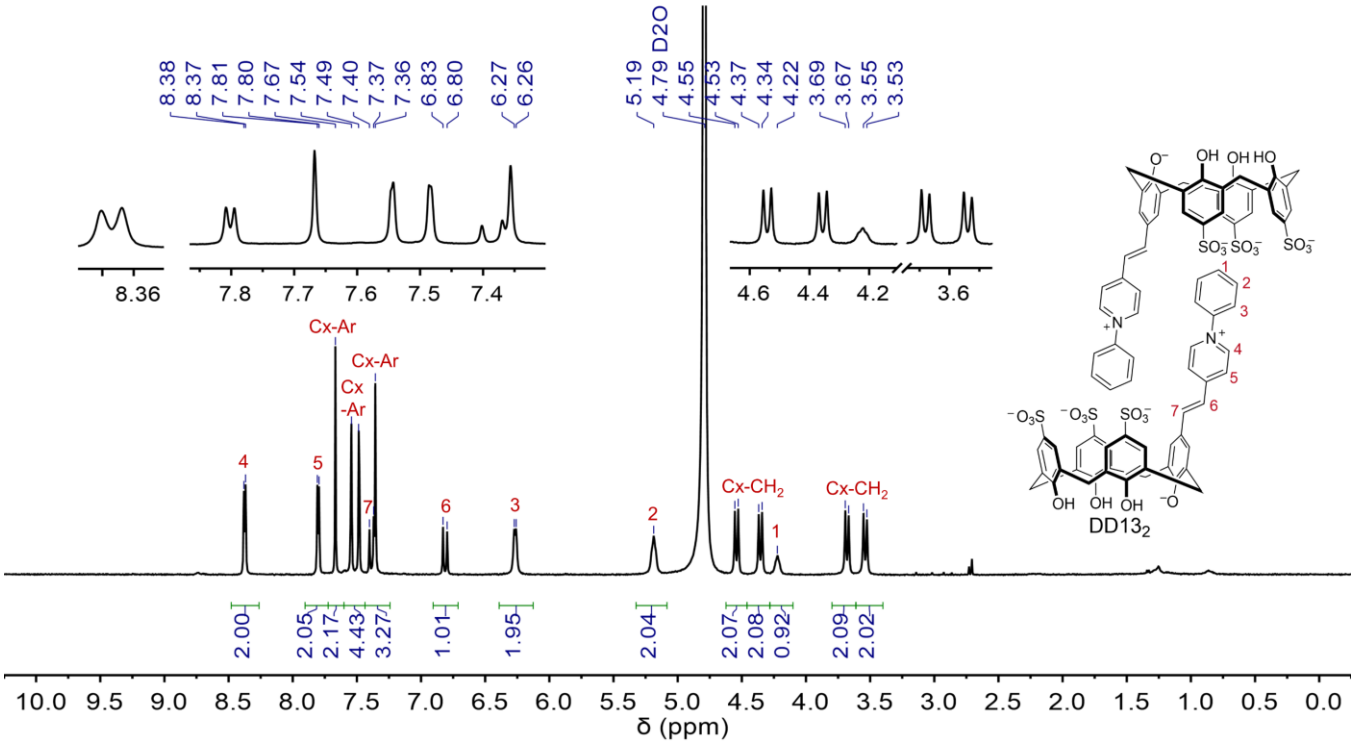

Figure S5. ^{1}H NMR spectrum of DD13$_2$ in NaH_2PO_4/Na_2HPO_4 (50 mM, pD 7.4) in D_2O (500 MHz, 298 K) shows upfield shifted pendant arm aromatic protons, supporting the existence of the molecule as a homodimer in aqueous solution.

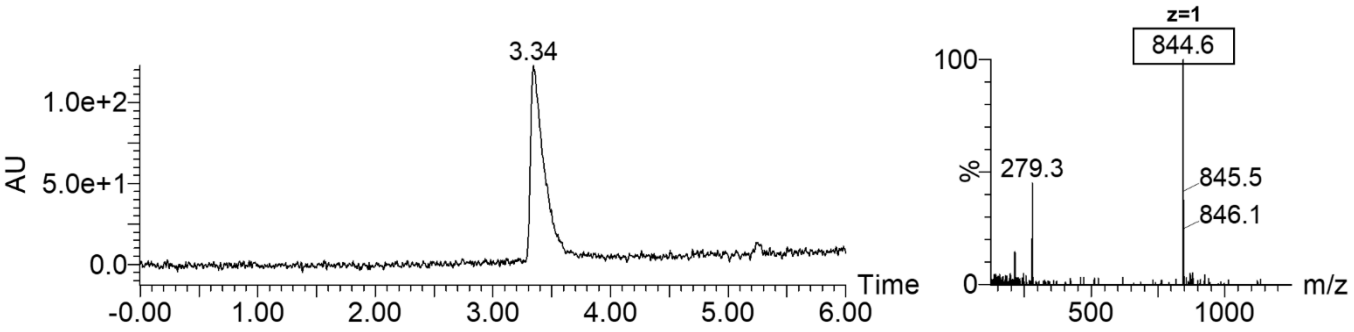

Figure S6. UPLC-MS (ES+) of DD13. Left = UV diode array detected chromatogram (190:800 nm). Right = positive ion mode ESI mass spectrum of the eluted peak.

Cucurbit[8]uril (CB8) was synthesized using literature methods.[2]

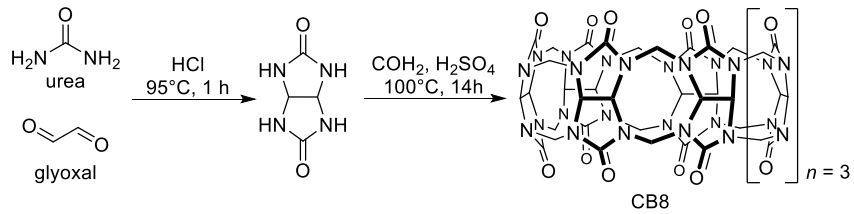

Scheme S2. Synthetic route of CB8.[2]

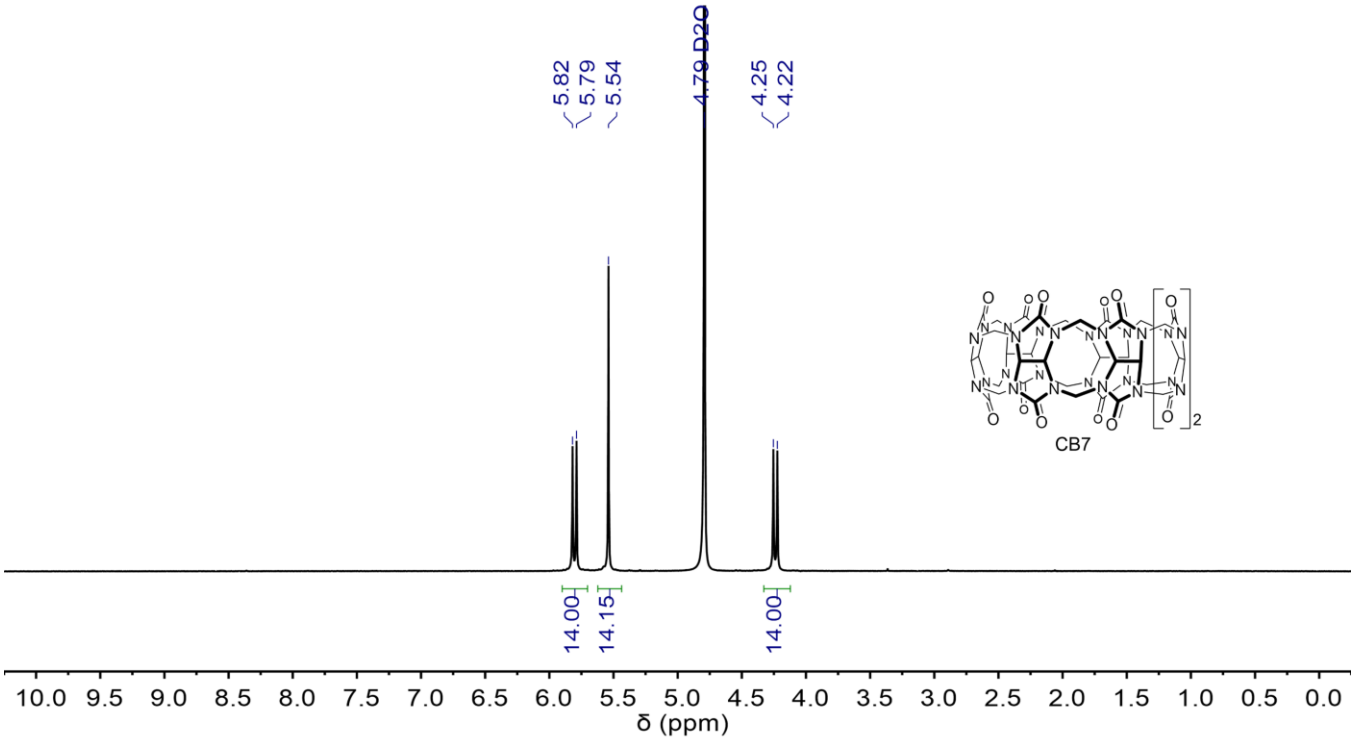

Figure S7. ^{1}H NMR spectrum of CB7 in D_2O (500 MHz, 298 K).

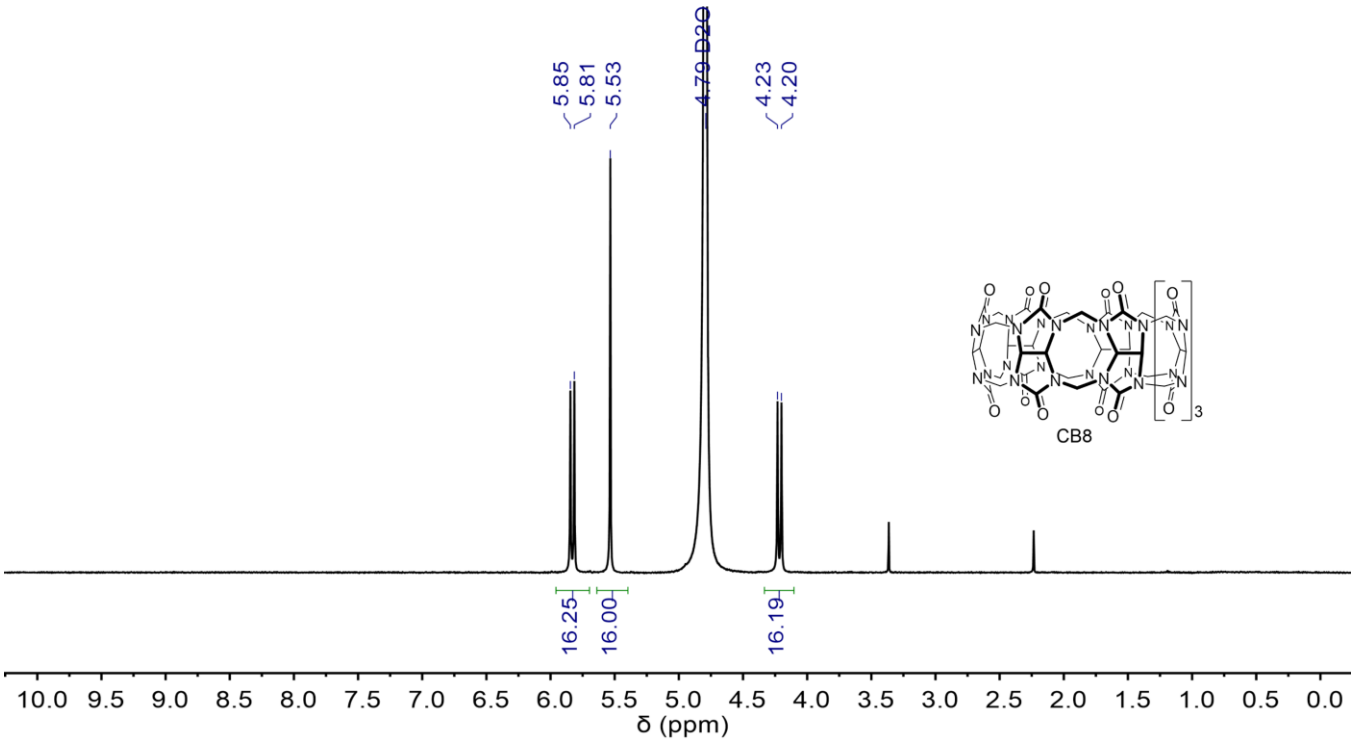

Figure S8. ^{1}H NMR spectrum of CB8 in D_2O (500 MHz, 298 K).

3. Mixed host co-assembled DimerDye•cucurbit[*n*]uril chemosensors

3.1. Cucurbit[*n*]uril into DimerDye titrations – absorbance and fluorescence

Preliminary experiments of a panel of previously reported DimerDyes (DD1, DD4, DD8, DD12 and DD13) with CB7 and CB8 were conducted, data not shown. DimerDyes in this work were narrowed down to DD4, DD8 and DD13 that showed changes in absorbance and/or fluorescence upon addition of CB7 or CB8.

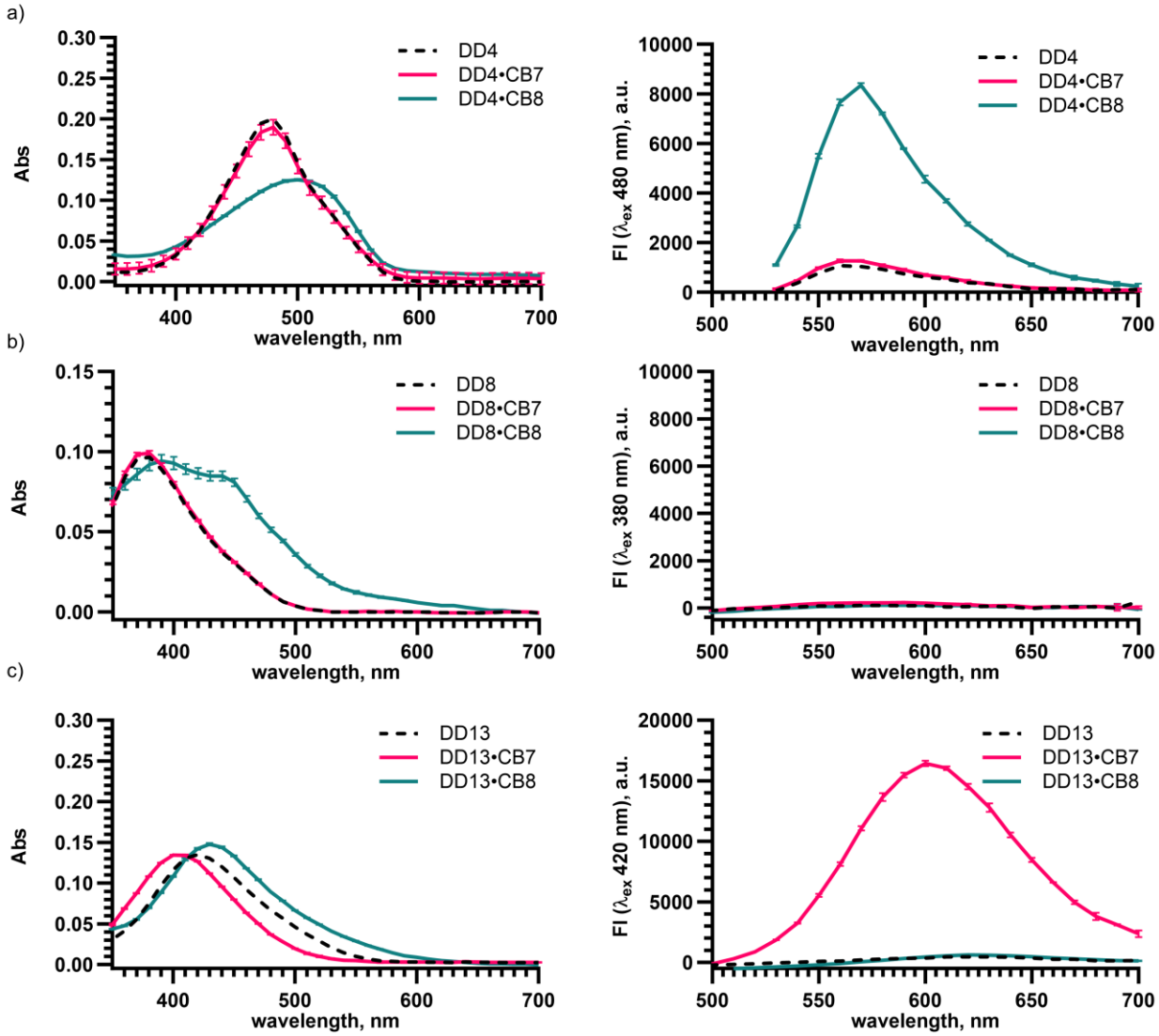

Figure S9. Select cucurbit[*n*]urils induce changes in DimerDye absorbance and fluorescence. a) DD4 produces a red shift in absorbance and turn-on fluorescence response with CB8. No change in DD4 absorbance or fluorescence is observed with CB7. b) DD8 produces a red shift in absorbance with CB8. No change in DD8 absorbance or fluorescence is observed with CB7. c) DD13 produces a blue shift in absorbance and turn-on fluorescence response with CB7 and a red shift in absorbance with CB8. Traces of DimerDyes (10.5 μM) alone are shown as black dashed lines. DimerDyes (10.5 μM) with CB7 (21 μM) are shown as red lines. DimerDyes (10.5 μM) with CB8 (21 μM) are shown as teal lines. All solutions in NaH_2PO_4/Na_2HPO_4 (10 mM, pH 7.4) in H_2O. Absorbance and fluorescence spectra are plotted as the mean of experiments done in triplicate with error bars corresponding to the standard deviation. Error bars are not visible in cases where the error is smaller than the depicted data point.

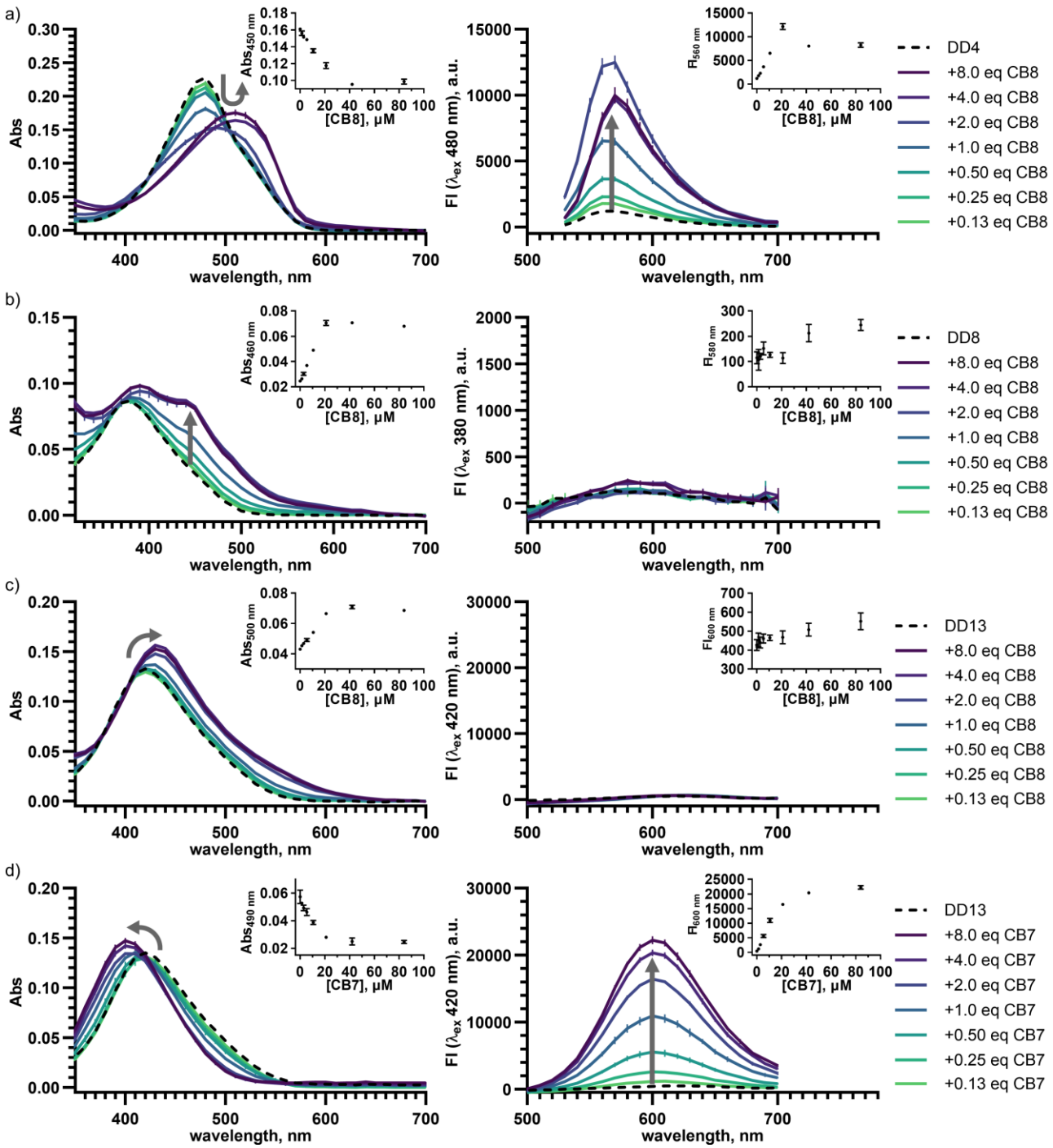

Figure S10. Titrations of cucurbit[*n*]uril into DimerDye induce red/blue shifts in absorbance and turn-on fluorescence responses. CB8 titrations into a) DD4 (10.5 μM) b) DD8 (10.5 μM) and c) DD13 (10.5 μM). CB7 titration into d) DD13 (10.5 μM). Titrations are monitored by absorbance (left) and fluorescence (right), where the darkest purple line represents the highest concentration of CB (84 μM) and the lightest green line represents the lowest concentration of CB (1.3 μM). Traces of DimerDyes (10.5 μM) alone are shown as black dashed lines. Insets show the binding isotherms. All solutions in NaH_2PO_4/Na_2HPO_4 (10 mM, pH 7.4) in H_2O. Absorbance and fluorescence spectra are plotted as the mean of experiments done in triplicate with error bars corresponding to the standard deviation. Error bars are not visible in cases where the error is smaller than the depicted data point.

Previous stopped-flow dimerization studies determined a dimer association constant (K_a) of (1.6 ± 0.9) × 10^5 M^{-1} for DD1 (1-methyl-pyridine analog).[17] Apparent dissociation constants ($K_{d,app}$) of DD•CB mixed host co-assembly were determined using absorbance binding isotherms, plotting the change in DimerDye absorbance (Abs-Abs_o) as a function of cucurbit[*n*]ruil concentration. The data was fit in GraphPad Prism using a direct one site binding equation, constrained by the constant concentration of DimerDye (10.5 μM):

$$Y = A \times \frac{(DD + x + K_{d,app}) - \sqrt{(DD + x + K_{d,app})^2 - (4DDx)}}{2DD}$$

Where, A = amplitude of change in absorbance (Abs-Abs_o),

DD = concentration of DimerDye

x = amount titrated

$K_{d,app}$ = apparent dissociation constant

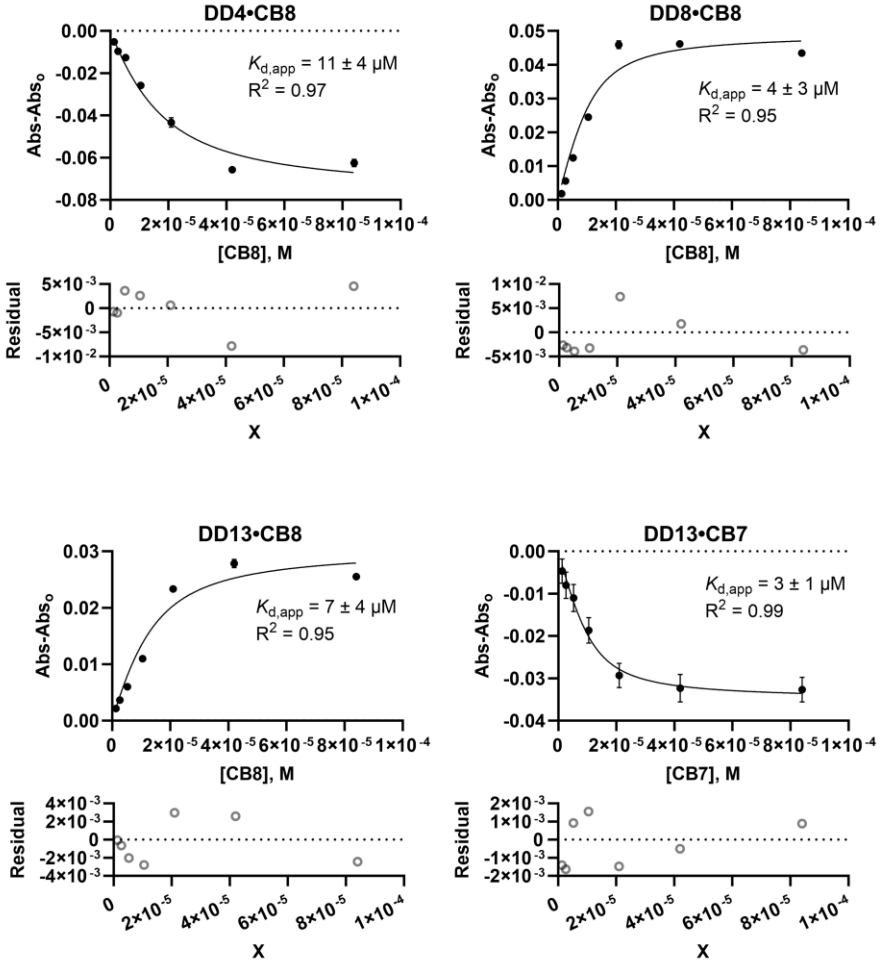

Figure S11. Apparent dissociation constants ($K_{d,app}$) of DimerDye•cucurbit[*n*]uril complexation determined from a direct one site binding model. Triplicate data from direct titrations of CB8 and CB7 into DimerDyes DD4, DD8 and DD13 (10.5 μM). Error bars were plotted for each triplicate but are not visible in cases where the error is smaller than the plotted point. All solutions in NaH_2PO_4/Na_2HPO_4 (10 mM, pH 7.4) in H_2O. Note: These fits do not account for the dissociation of the dimer and should only be considered as comparisons between related systems.

3.2. ^{1}H NMR investigation of mixed host co-assembled DD•CB chemosensor complexes

^{1}H NMR experiments were conducted to further validate DD•CB complexation interactions. Studies were limited by the solubility restraints of DD•CB complexes at concentrations required for ^{1}H NMR studies. Therefore, only mixed host complexation interactions of DD4•CB8 and DD13•CB7 were investigated by ^{1}H NMR. The turn-off fluorescence sensing mechanism of DD13•CB7 was further probed by ^{1}H NMR through the addition of a CB7 selective guest ($AdNH_3^+$). These solubility limitations prevented further experimental investigation of the size of complexes formed by dynamic light scattering (DLS) or diffusion ordered spectroscopy (DOSY).

Stock solutions of cucurbit[*n*]uril hosts (CB7 and CB8) were prepared in D_2O and concentrations were determined by titration experiments with known strong binding dyes (MDAP and BC, respectively) in H_2O.[13, 14] Stock solutions of DimerDyes (1 mM) were prepared by mass in NaH_2PO_4/Na_2HPO_4 (50 mM, pD 7.4) in D_2O. Final NMR solutions contained [DD] = 100 µM, [CB] = 100 µM in NaH_2PO_4/Na_2HPO_4 (10 mM, pD 7.4) in D_2O.

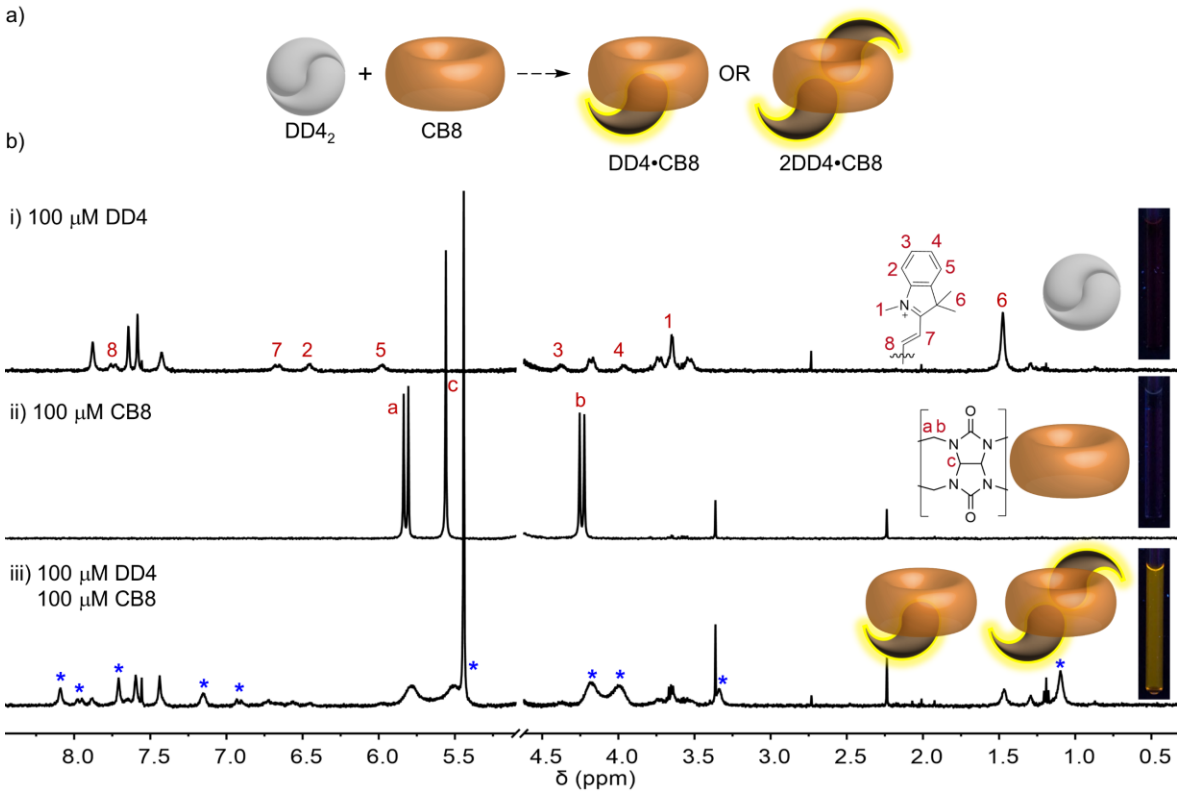

Figure S12. DD4 and CB8 form a fluorescent mixed host chemosensor. a) Schematic of DD4•CB8 co-assembly illustrating possible binary and ternary complexes that could form in the larger CB8 cavity.[18-20] b) ^{1}H NMR of i) DD4 (100 µM). Upfield-shifted aromatic peaks in fast exchange and non-fluorescent appearance support the existence of the homodimer $DD4_2$ in aqueous solution. ii) CB8 (100 µM). iii) DD4 (100 µM) and CB8 (100 µM) combined. Blue stars illustrate the appearance of new DD4 and CB8 resonances. The presence of new upfield-shifted and broadened aromatic peaks and upfield-shifted methyl peaks indicate DD4•CB8 complexation. Fluorescent appearance of the NMR tube further supports the disassembly of the homodimer $DD4_2$. NMR tube irradiated with a hand-held UV lamp (λ_{ex} = 356±20 nm). All samples in NaH_2PO_4/Na_2HPO_4 (10 mM, pD 7.4) in D_2O (500 MHz, 298 K).

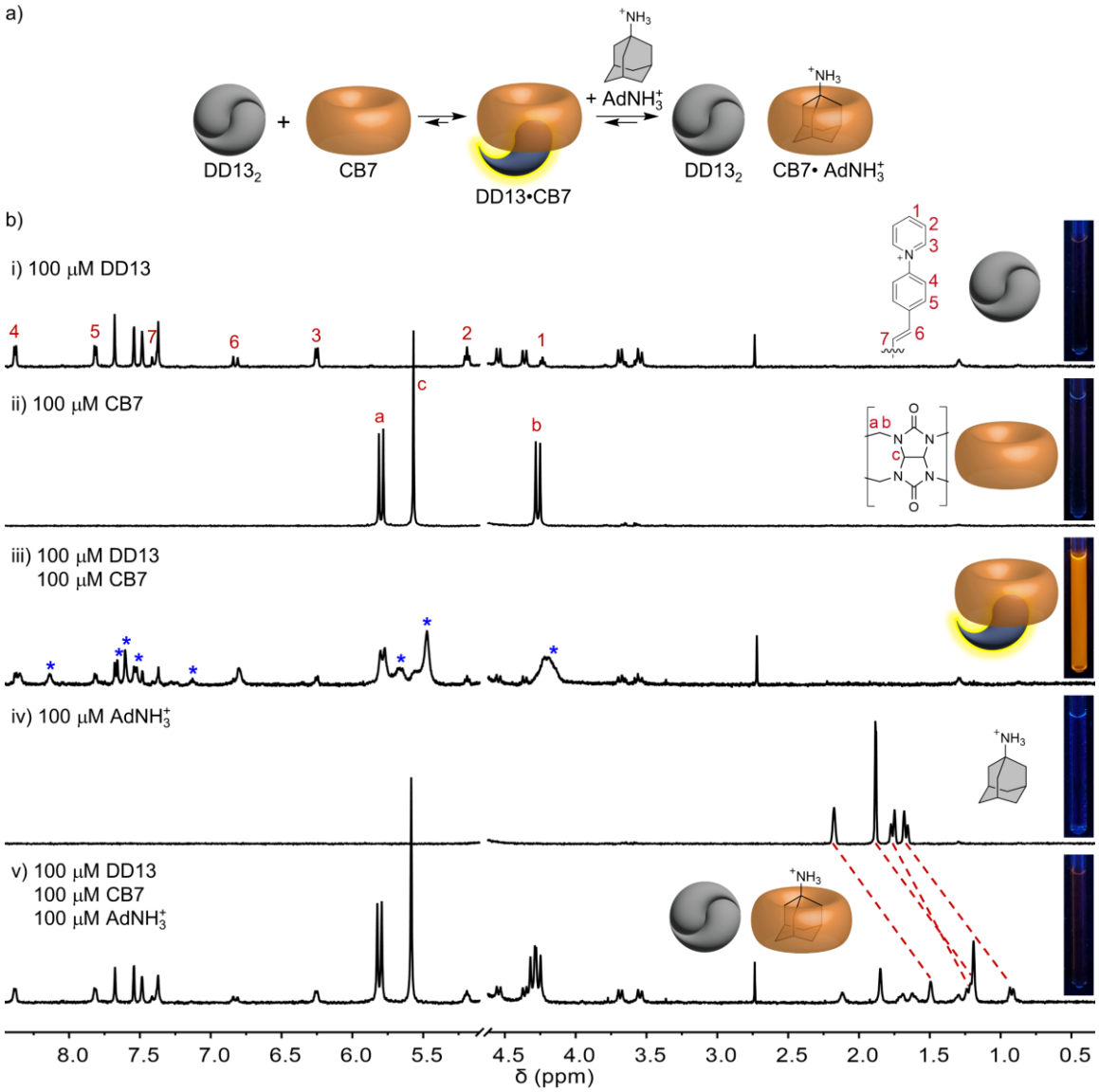

Figure S13. DD13•CB7 complex functions as a turn-off mixed host chemosensor for strong binding guests of CB7. a) Schematic of DD13•CB7 formation and turn-off sensing mechanism upon analyte addition. b) ^{1}H NMR of i) DD13 (100 μM) shows upfield-shifted aromatic peaks in fast exchange. Non-fluorescent appearance of the NMR tube supports the existence of homodimer DD13$_2$ in aqueous solution. ii) CB7 (100 μM). iii) DD13 (100 μM) and CB7 (100 μM) combined. Blue stars illustrate the appearance of new DD13 and CB7 resonances. The presence of new upfield-shifted and broadened aromatic peaks indicate DD4•CB8 complexation. The fluorescent appearance of the NMR tube further supports the disassembly of the homodimer DD13$_2$. iv) AdNH$_3^+$ (100 μM). v) DD13 (100 μM), CB7 (100 μM) and AdNH$_3^+$ (100 μM) combined. Upfield-shifted AdNH$_3^+$ peaks (red dashed lines) and the return of homodimer DD13$_2$ peaks indicate a CB7•AdNH$_3^+$ assembly forms. The non-fluorescent appearance of the NMR tube further supports the reformation of the homodimer DD13$_2$. NMR tube irradiated with a hand-held UV lamp (λ_{ex} 356±20 nm). All samples in NaH_2PO_4/Na_2HPO_4 (10 mM, pD 7.4) in D_2O (500 MHz, 298 K).

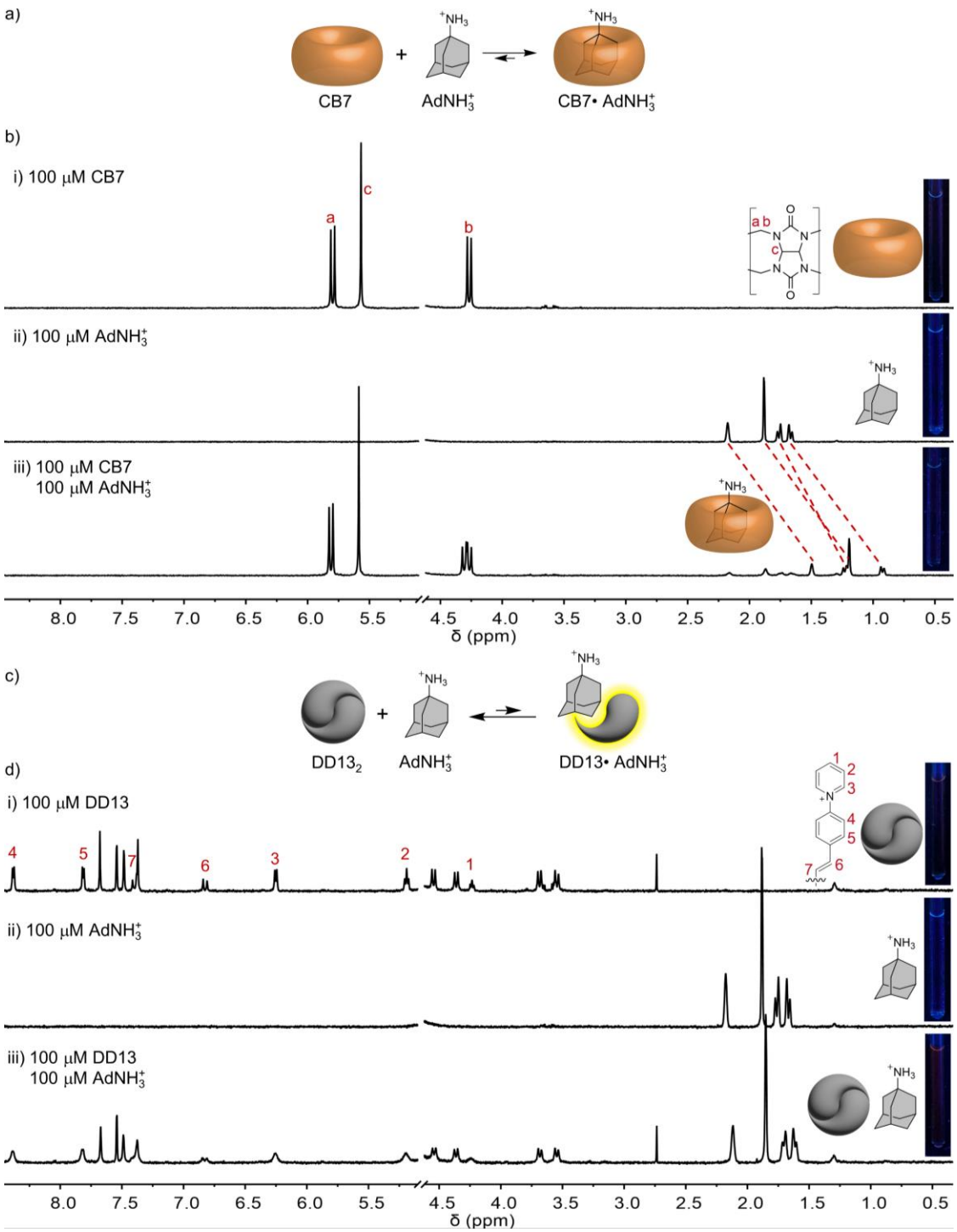

Figure S14. Control experiments demonstrate that the DD13•CB7 mixed host complex is responsible for observed sensing responses. a) Schematic illustrating CB7•$AdNH_3^+$ favored complexation. b) ^{1}H NMR of i) CB7 (100 μM) ii) $AdNH_3^+$ (100 μM) and iii) CB7 (100 μM) combined with $AdNH_3^+$ (100 μM). Complexation of $AdNH_3^+$ is observed by upfield-shifted resonances in slow exchange, shown as red dashed lines. All NMR tubes are non-fluorescent in appearance as CB7 and $AdNH_3^+$ are spectroscopically silent. c) Schematic illustrating the homodimer $DD13_2$ is favored over DD13•$AdNH_3^+$ complexation. d) ^{1}H NMR of i) DD13 (100 μM), upfield-shifted aromatic peaks in fast exchange and non-fluorescent appearance supports the existence of homodimer $DD13_2$ in aqueous solution. ii) $AdNH_3^+$ (100 μM). iii) DD13 (100 μM) and $AdNH_3^+$ (100 μM) combined. Minimal shifts observed in $AdNH_3^+$ and $DD13_2$ resonances indicate little disruption of the $DD13_2$ homodimer. The non-fluorescent appearance of the NMR tube further supports the presence of $DD13_2$ homodimer. NMR tube irradiated with a hand-held UV lamp (λ_{ex} = 356±20 nm). All samples in NaH_2PO_4/Na_2HPO_4 (10 mM, pD 7.4) in D_2O (500 MHz, 298 K).

3.3. Molecular modeling of DD13•CB7 co-assembly

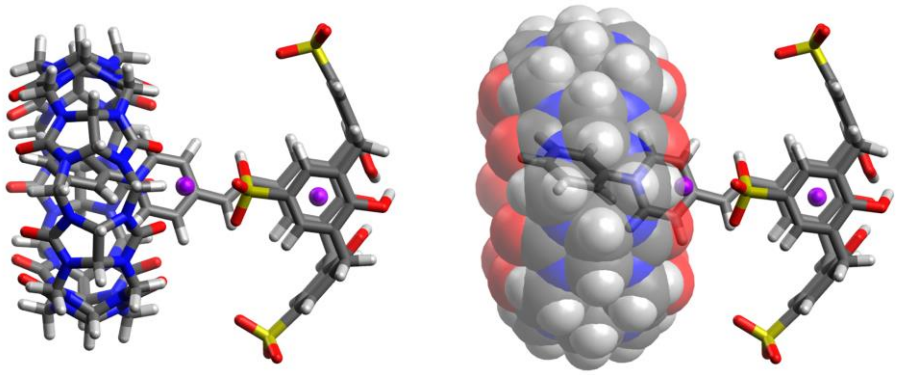

Figure S15. Molecular modeling using DFT (RWB97X-D/6-31G(D)) was performed with Spartan to illustrate a potential 1:1 binding geometry between DD13 and CB7. To partially counterbalance the overall charge of the complex, two sodium ions were strategically placed: one within the DD13 cavity, which is recognized for its Na+ binding capability, and another adjacent to the CB7 portals, known for their cation-binding affinity.[21] It is important to note that, in reality, a variety of conformers likely exist, differing in both the number and positions of bound counterions. Therefore, this molecular model should be viewed as a visual representation intended to provide insight into possible binding configurations, rather than a definitive structural depiction.

4. DimerDye and mixed host co-assembly titrations with cocaine

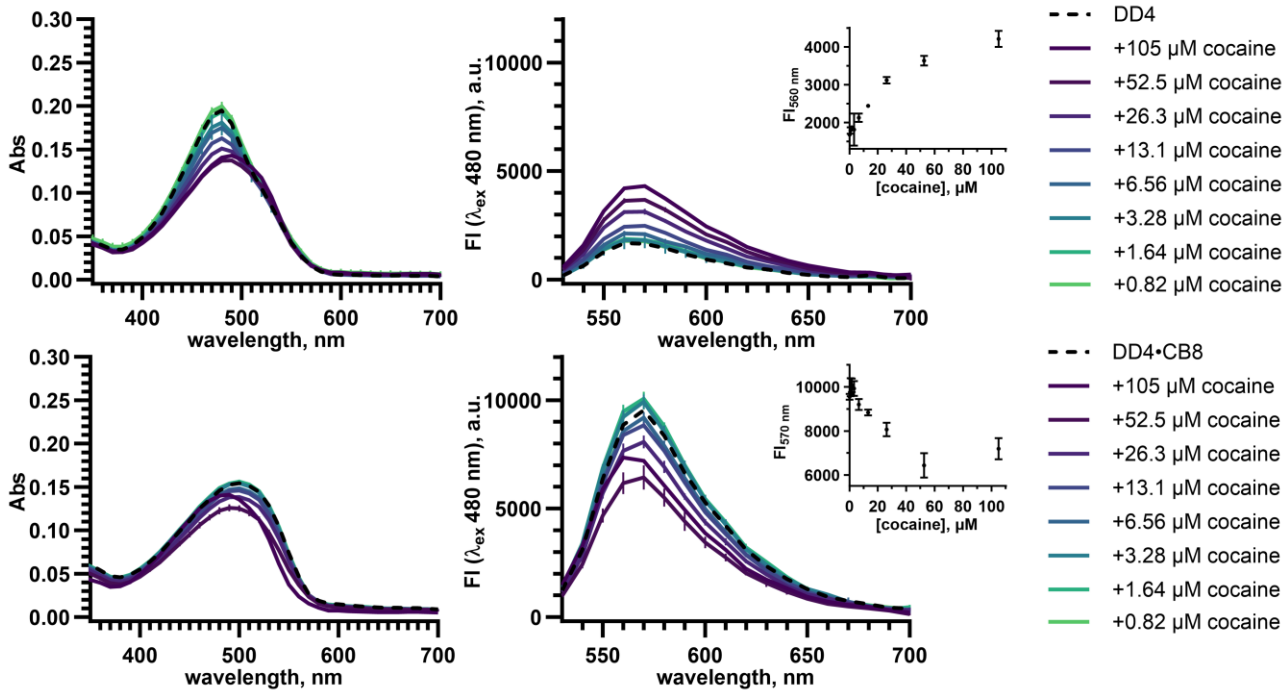

Figure S16. Titrations of cocaine into DD4 (top) and cocaine into DD4•CB8 (bottom). Titrations monitored by absorbance and fluorescence, where the darkest purple line represents the highest concentration of cocaine (105 μM) and the lightest green line represents the lowest concentration of cocaine (0.82 μM). Traces of DimerDye ([DD4] = 10.5 μM) or DD4•CB8 ([DD4] = 10.5 μM, [CB8] = 21 μM) alone are shown as black dashed lines. Insets show the fluorescence binding isotherms. All solutions in NaH_2PO_4/Na_2HPO_4 (8.4 mM, pH 7.4) in H_2O with 2% MeOH. Absorbance and fluorescence spectra are plotted as the mean of experiments done in triplicate with error bars corresponding to the standard deviation. Error bars are not visible in cases where the error is smaller than the depicted data point.

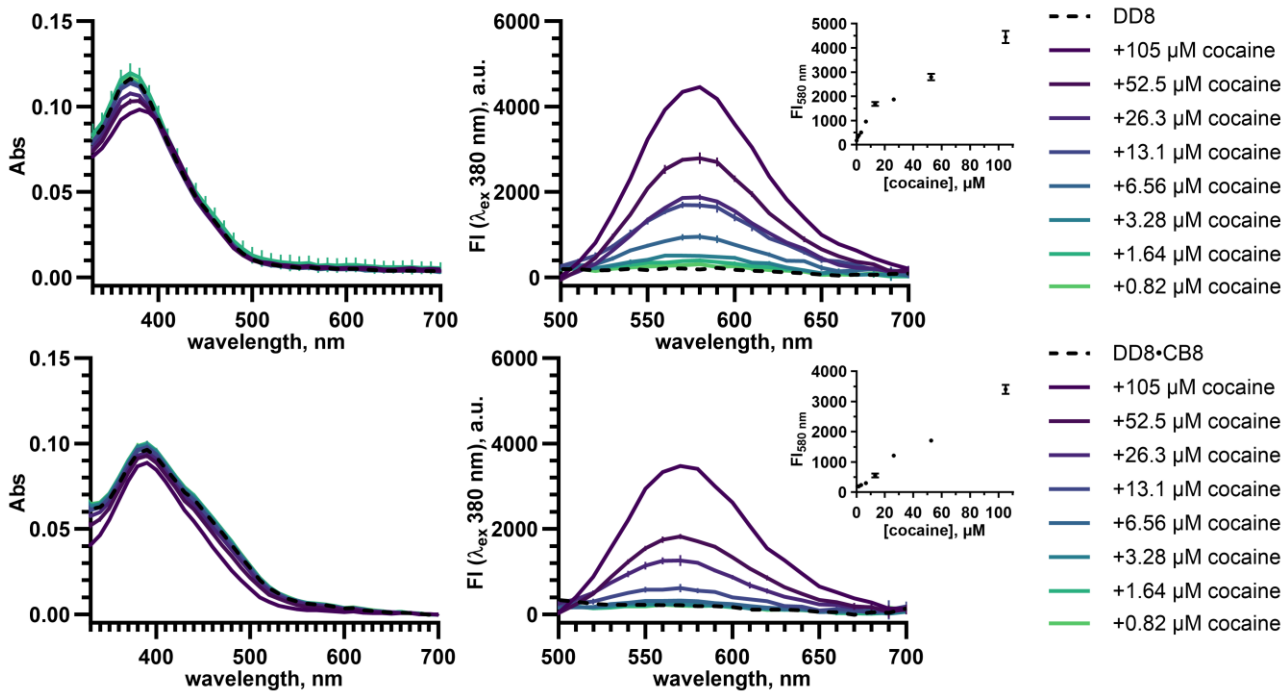

Figure S17. Titrations of cocaine into DD8 (top) and cocaine into DD8•CB8 (bottom). Titrations monitored by absorbance and fluorescence, where the darkest purple line represents the highest concentration of cocaine (105 μM) and the lightest green line represents the lowest concentration of cocaine (0.82 μM). Traces of DimerDye ([DD8] = 10.5 μM) or DD8•CB8 ([DD8] = 10.5 μM, [CB8] = 21 μM) alone are shown as black dashed lines. Insets show the fluorescence binding isotherms. All solutions in NaH_2PO_4/Na_2HPO_4 (8.4 mM, pH 7.4) in H_2O with 2% MeOH. Absorbance and fluorescence spectra are plotted as the mean of experiments done in triplicate with error bars corresponding to the standard deviation. Error bars are not visible in cases where the error is smaller than the depicted data point.

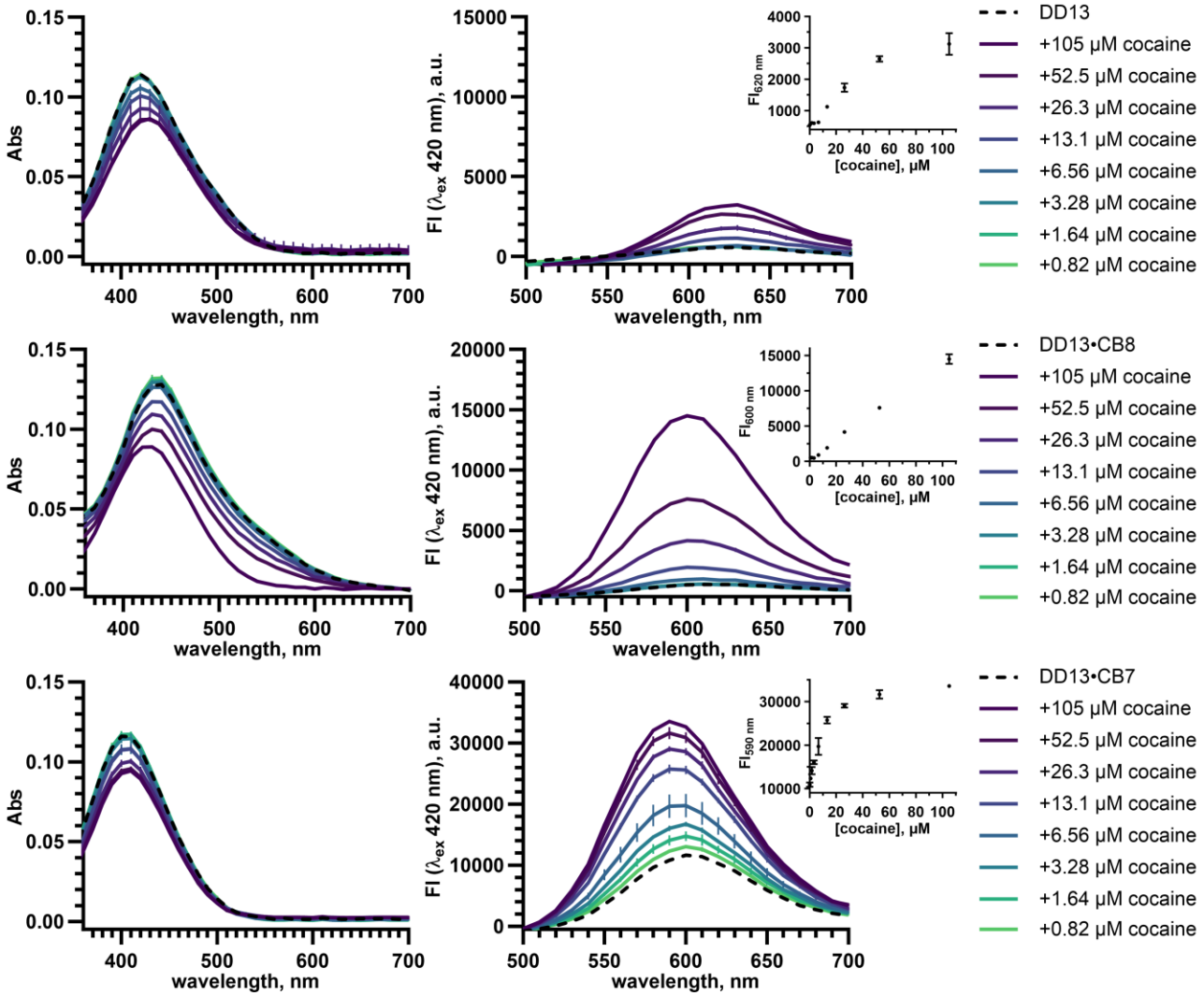

Figure S18. Titrations of cocaine into DD13 (top), cocaine into DD13•CB8 (middle) and cocaine into DD13•CB7 (bottom). Titrations monitored by absorbance and fluorescence, where the darkest purple line represents the highest concentration of cocaine (105 μM) and the lightest green line represents the lowest concentration of cocaine (0.82 μM). Traces of DimerDye ([DD13] = 10.5 μM), DD13•CB8 ([DD13] = 10.5 μM, [CB8] = 21 μM) and DD13•CB7 ([DD13] = 10.5 μM, [CB7] = 21 μM) alone are shown as black dashed lines. Insets show the fluorescence binding isotherms. All solutions in NaH_2PO_4/Na_2HPO_4 (8.4 mM, pH 7.4) in H_2O with 2% MeOH. Absorbance and fluorescence spectra are plotted as the mean of experiments done in triplicate with error bars corresponding to the standard deviation. Error bars are not visible in cases where the error is smaller than the depicted data point.

Limits of detection (LODs) were determined by fitting a linear regression to the linear region of each cocaine titration curve and calculating $LOD = \frac{3.3\sigma}{m}$, where σ is the standard deviation of the y-intercept and m is the slope of the linear regression.[22]

Table S1. LODs of cocaine with DimerDye and mixed host co-assembled chemosensors in NaH_2PO_4/Na_2HPO_4 (8.4 mM, pH 7.4) in H_2O with 2% MeOH.

Chemosensor	σ	m	LOD (μM)
DD4	45.1	53.6	2.78
DD4•CB8	202	-184	3.62
DD8	17.9	114	0.51
DD8•CB8	24.7	30.9	2.64
DD13	25.7	41.5	2.05
DD13•CB8	66.1	136	1.60
DD13•CB7	340	1106	1.02

5. Princial Component Analysis

PCA analysis was conducted using a combination of select absorbance and fluorescence wavelength responses. The general process for PCA analysis is described below. A detailed tutorial review providing methods on improving visual discrimination is reported by Anslyn et al.[23]

- Spectral scans of chemosensor absorbance and fluorescence responses to different analytes were visually compared. Key individual wavelengths that provided separated patterns of response, different/unique patterns and large amplitudes in change were initially selected (e.g. absorbance and fluorescence maxima of each chemosensor and wavelengths that capture induced shifts in maxima).
- PCA analysis was done using the selected wavelength responses, producing loading plots that identify the vector contribution of each chemosensor wavelength.
- Loading plots were evaluated and chemosensor responses were narrowed down to provide the most discrimination. This was done through an iterative process of PCA and loading plot re-evaluation; eliminating chemosensor vectors with small or close to zero contribution, eliminating unnecessary overlapping vectors (chemosensors with redundant sensing patterns) and maximizing overall vector separation.

5.1. Identifying illicit drugs and adulterants

Discriminant analysis experiments of illicit drugs and adulterants were conducted in NUNC black-walled optical bottom 384-well plates, with 70 μL final well volumes. Final solutions contained [DD] = 10.5 μM, [CB] = 21 μM, and [drug] = 105 μM in NaH_2PO_4/Na_2HPO_4 (8.4 mM, pH 7.4) in H_2O with 2% MeOH. Mixed host chemosensor combinations of DD4•CB8, DD8•CB8, DD13•CB8, and DD13•CB7 were tested for their responses to each individual illicit drug and adulterant. Absorbance and emission wavelengths were selected based on preliminary experimental results, using excitation wavelengths at the maxima of each DimerDye (DD4 λ_{ex} = 480 nm, DD8 λ_{ex} = 380 nm and DD13 λ_{ex} = 420 nm) (Table S1). Cannabinoid sensing of DimerDyes alone was also tested using the same selected absorbance and fluorescence wavelengths (Table S2), this was done to validate the improved differentiation ability of the array of mixed host chemosensors. Absorbance and fluorescence end-point measurements of each DD•CB•drug combination were collected in 12 replicates, along with 2 solvent blank measurements. The raw data was pre-processed by subtracting the solvent blank from each DD•CB•drug measurement, then the two highest and two lowest data values were systematically excluded. Absorbance and fluorescence wavelengths that provided discrimination of drugs and adulterants were selected for PCA, while aiming to minimize the number of observations. PCA correlation plots with confidence ellipses (95%) and loading vectors were plotted on sample sets of 8 replicates using OriginPro 2022b Principal Component Analysis App (Version: 1.50, File Name: PCAC.opx).

Table S2. Mixed host chemosensor wavelengths used in PCA analysis for the identification of drugs and adulterants.

Mixed host chemosensor	Absorbance (nm)	Fluorescence (λ_{ex} (nm), λ_{em} (nm))
DD4•CB8	480	480, 570 480, 600
DD8•CB8	440	380, 570
DD13•CB8	400 430	420, 600
DD13•CB7	400 430	420, 600

Table S3. DimerDye chemosensor wavelengths used in PCA analysis for the identification of cannabinoids.

DimerDye	Absorbance (nm)	Fluorescence (λ_{ex} (nm), λ_{em} (nm))
DD4	480	480, 570 480, 600
DD8	440	380, 570
DD13	400 430	420, 600

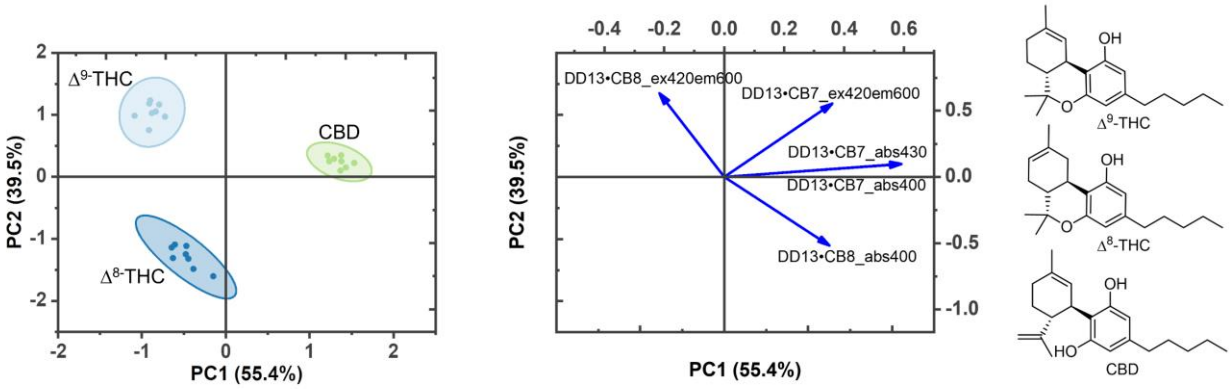

Figure S19. An array of mixed host chemosensors differentiates structurally similar neutral cannabinoids. Sensor array includes absorbance and fluorescence responses of mixed host chemosensors DD13•CB7 and DD13•CB8. PCA (correlation) score plot shows each sample set (n = 8) enclosed by 95% confidence ellipses with the respective loading plot of absorbance and fluorescence variables shown as blue vectors. Chemical structures are represented in the expected protonation forms under sensing conditions of pH 7.4. Samples contain [DD] = 10.5 μM, [CB] = 21 μM and [drug] = 105 μM. All samples are in NaH_2PO_4/Na_2HPO_4 (8.4 mM, pH 7.4) in H_2O with 2% MeOH.

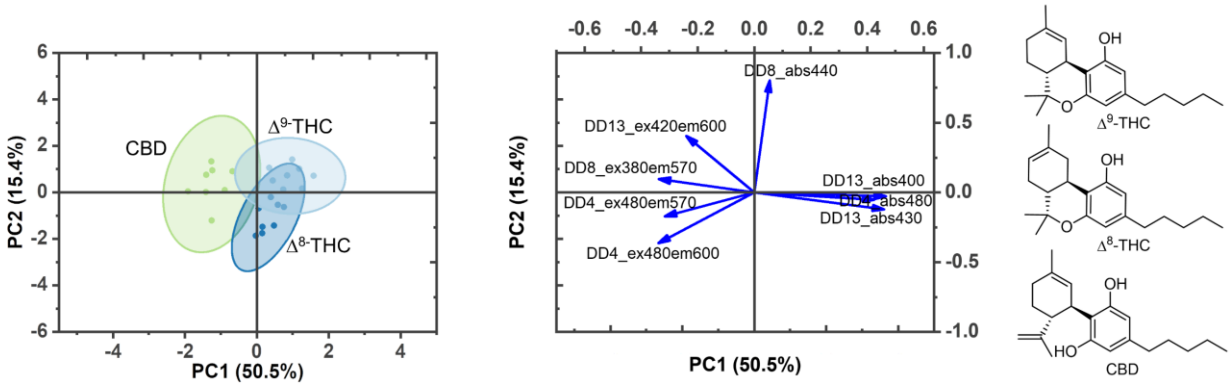

Figure S20. An array of DimerDye chemosensors does not differentiate structurally similar neutral cannabinoids. Sensor array includes absorbance and fluorescence responses of DD4, DD8, and DD13. PCA (correlation) score plot shows each sample set (n = 8) enclosed by 95% confidence ellipses with the respective loading plot of absorbance and fluorescence variables shown as blue vectors. Chemical structures are represented in the expected protonation forms under sensing conditions of pH 7.4. Samples contain [DD] = 10.5 μM and [drug] = 105 μM. All samples are in NaH_2PO_4/Na_2HPO_4 (8.4 mM, pH 7.4) in H_2O with 2% MeOH.

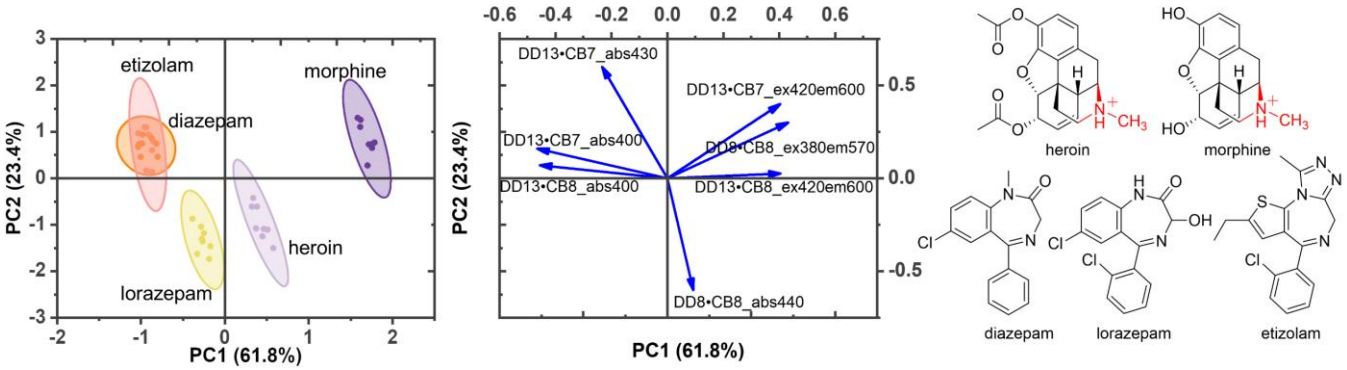

Figure S21. An array of mixed host chemosensors shows the differentiation of Central Nervous System (CNS) depressant cationic opiates and neutral benzodiazepine analogs. Sensor array includes absorbance and fluorescence responses of mixed host chemosensors DD8•CB8, DD13•CB8, and DD13•CB7. PCA (correlation) score plot shows each sample set (n = 8) enclosed by 95% confidence ellipses with the respective loading plot of absorbance and fluorescence variables shown as blue vectors. Chemical structures are represented in the expected protonation forms under sensing conditions of pH 7.4. Samples contain [DD] = 10.5 μM, [CB] = 21 μM, [drug] = 105 μM. All samples are in NaH_2PO_4/Na_2HPO_4 (8.4 mM, pH 7.4) in H_2O with 2% MeOH.

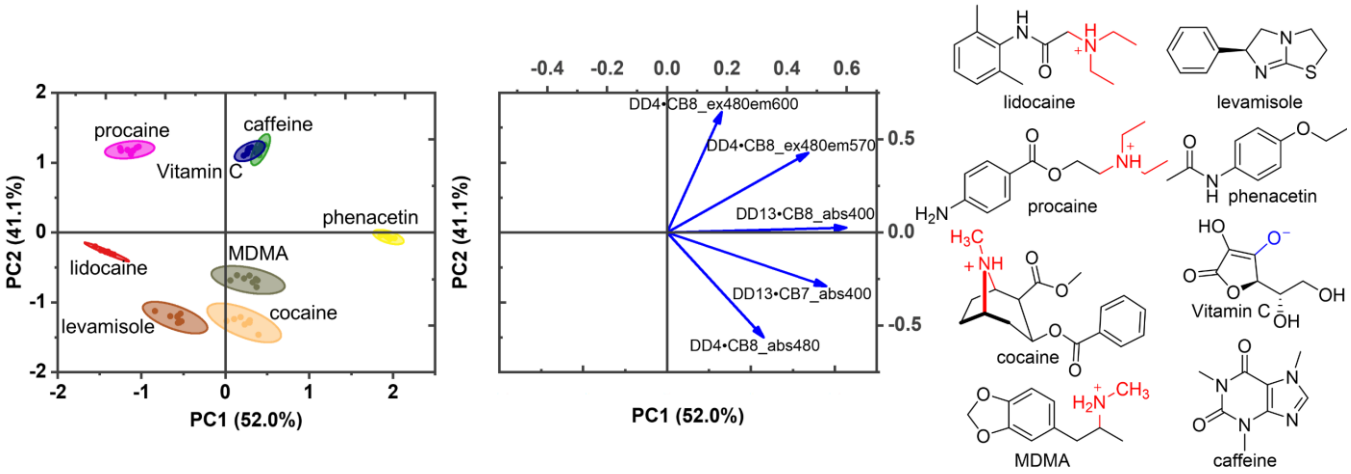

Figure S22. An array of mixed host chemosensors discriminates anesthetics and amphetamine from common adulterants. Sensor array includes absorbance and fluorescence responses of mixed host chemosensors DD4•CB8, DD13•CB8, and DD13•CB7. PCA (correlation) score plot shows each sample set (n = 8) enclosed by 95% confidence ellipses with the respective loading plot of absorbance and fluorescence variables shown as blue vectors. Chemical structures are represented in the expected protonation forms under sensing conditions of pH 7.4. Samples contain [DD] = 10.5 µM, [CB] = 21 µM and [drug] = 105 µM. All samples are in NaH_2PO_4/Na_2HPO_4 (8.4 mM, pH 7.4) in H_2O with 2% MeOH.

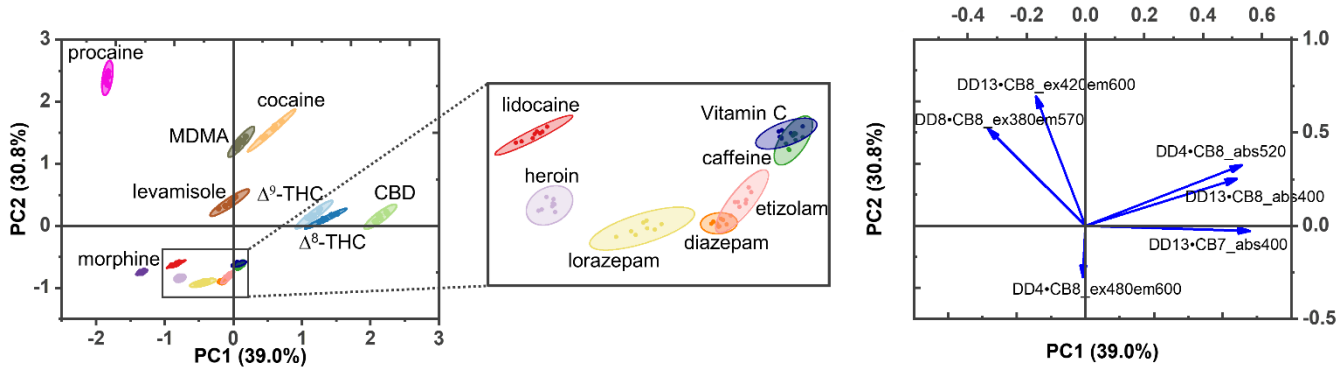

Figure S23. All drug and adulterant differentiation from an array of mixed host chemosensors. Sensor array includes absorbance and fluorescence responses from mixed host chemosensors DD4•CB8, DD8•CB8, DD13•CB8, and DD13•CB7. PCA (correlation) score plot shows each sample set (n = 8) enclosed by 95% confidence ellipses with the respective loading plot of absorbance and fluorescence observations shown as blue arrows. Samples contain [DD] = 10.5 µM, [CB] = 21 µM, [drug] = 105 µM. All samples are in NaH_2PO_4/Na_2HPO_4 (8.4 mM, pH 7.4) in H_2O with 2% MeOH.

5.2. Identifying multi-component street drug samples

Discriminant analysis experiments of multi-component street drug samples were conducted in NUNC black-walled optical bottom 384-well plates, with 50 µL final well volumes. Final solutions contained [DD] = 10.5 µM, [CB] = 21 µM, [street drug sample] = 0.03 mg/mL in NaH_2PO_4/Na_2HPO_4 (8.4 mM, pH 7.4) in H_2O with 2% MeOH. A blank of each multi-component street drug sample was measured to ensure no signal overlap in the DimerDye regions. Full absorbance and fluorescence spectral scans of each combination were collected in 12 replicates, along with 2 solvent blank measurements. Full spectral scans were collected to cover any binding induced changes in λ_{max} occurring in the multi-component mixtures (Figure S19 and S20). Excitation wavelengths were selected at the maxima of each DimerDye (DD4 λ_{ex} = 480 nm, DD8 λ_{ex} = 380 nm, DD13 λ_{ex} = 420 nm). A second set of absorbance spectral scans was taken after the experiment was completed and compared to the measurements from the start of the experiment, this was done to ensure there were no changes in the spectra throughout the course of experimental measurements and a steady equilibrium was reached within the multi-component mixtures. Collected raw data was preprocessed by subtracting a buffer blank from absorbance and fluorescence readings. Absorbance and fluorescence wavelengths from the mixed host chemosensors that provided different responses to the multi-component street drug samples were selected for PCA discrimination, while aiming to use a minimal number of observations (Table S3). DimerDye chemosensors alone were also tested using the same selected absorbance and fluorescence wavelengths (Table S4) as a direct comparison of the DimerDye sensor array (Figure S22) to the array of DD•CB mixed host chemosensors (Figure S21). PCA correlation plots with confidence ellipses (95%) and loading vectors were plotted on sample sets of 8 replicates using OriginPro 2022b Principal Component Analysis App (Version: 1.50, File Name: PCAC.opx).

Table S4. Mixed host chemosensor wavelengths used in PCA analysis for the identification of multi-component street drug samples.

Mixed host chemosensor	Absorbance (nm)	Fluorescence ($\lambda_{ex.}$ nm, $\lambda_{em.}$ nm)
DD4•CB8	-	480, 570 480, 580
DD8•CB8	-	380, 580
DD13•CB8	430	420, 600
DD13•CB7	400	420, 600

Table S5. DimerDye chemosensor wavelengths used in PCA analysis for the identification of multi-component street drug samples.

DimerDye	Absorbance (nm)	Fluorescence ($\lambda_{ex.}$ nm, $\lambda_{em.}$ nm)
DD4	-	480, 570 480, 580
DD8	-	380, 580
DD13	400 430	420, 600

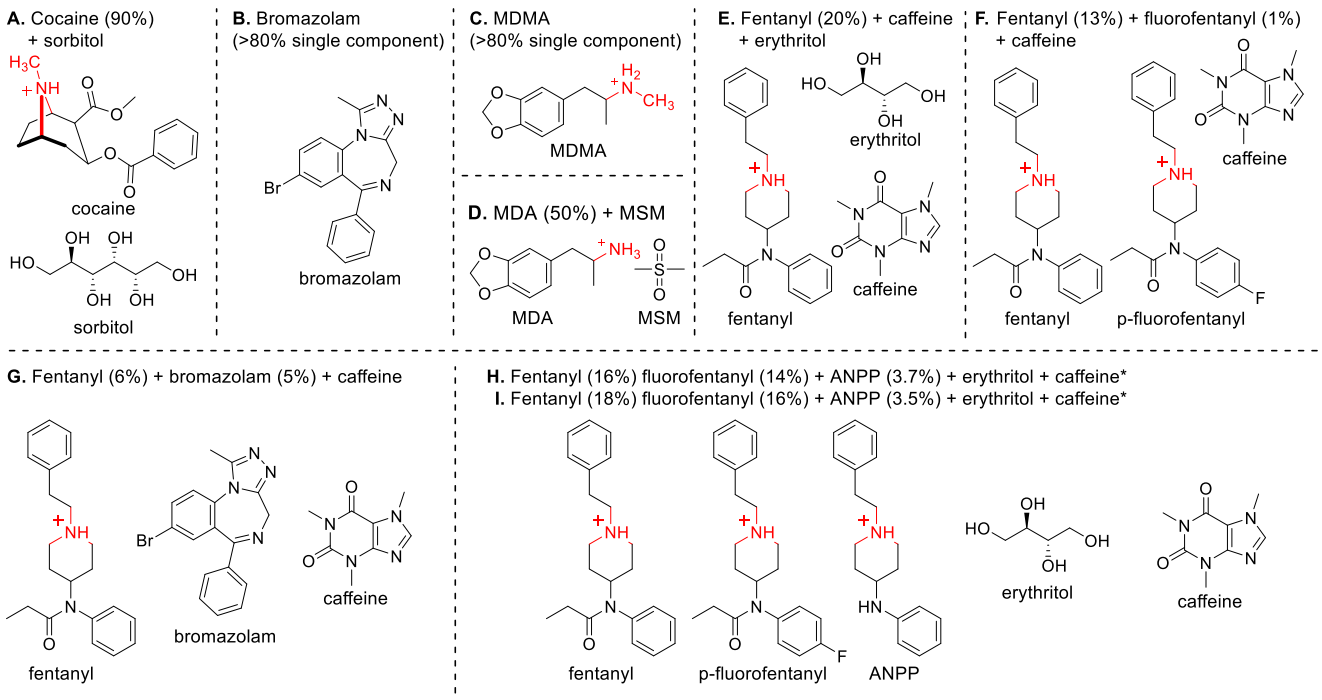

Figure S24. Composition and chemical structures of the multi-component street drug samples A-I acquired through Substance, the Vancouver Island Drug Checking Project, located in Victoria, British Columbia, Canada.[5] *Samples H and I were provided by two different people reporting the same drug from the same batch and supplier. All chemical structures are represented in the expected protonation forms under sensing conditions of pH 7.4.

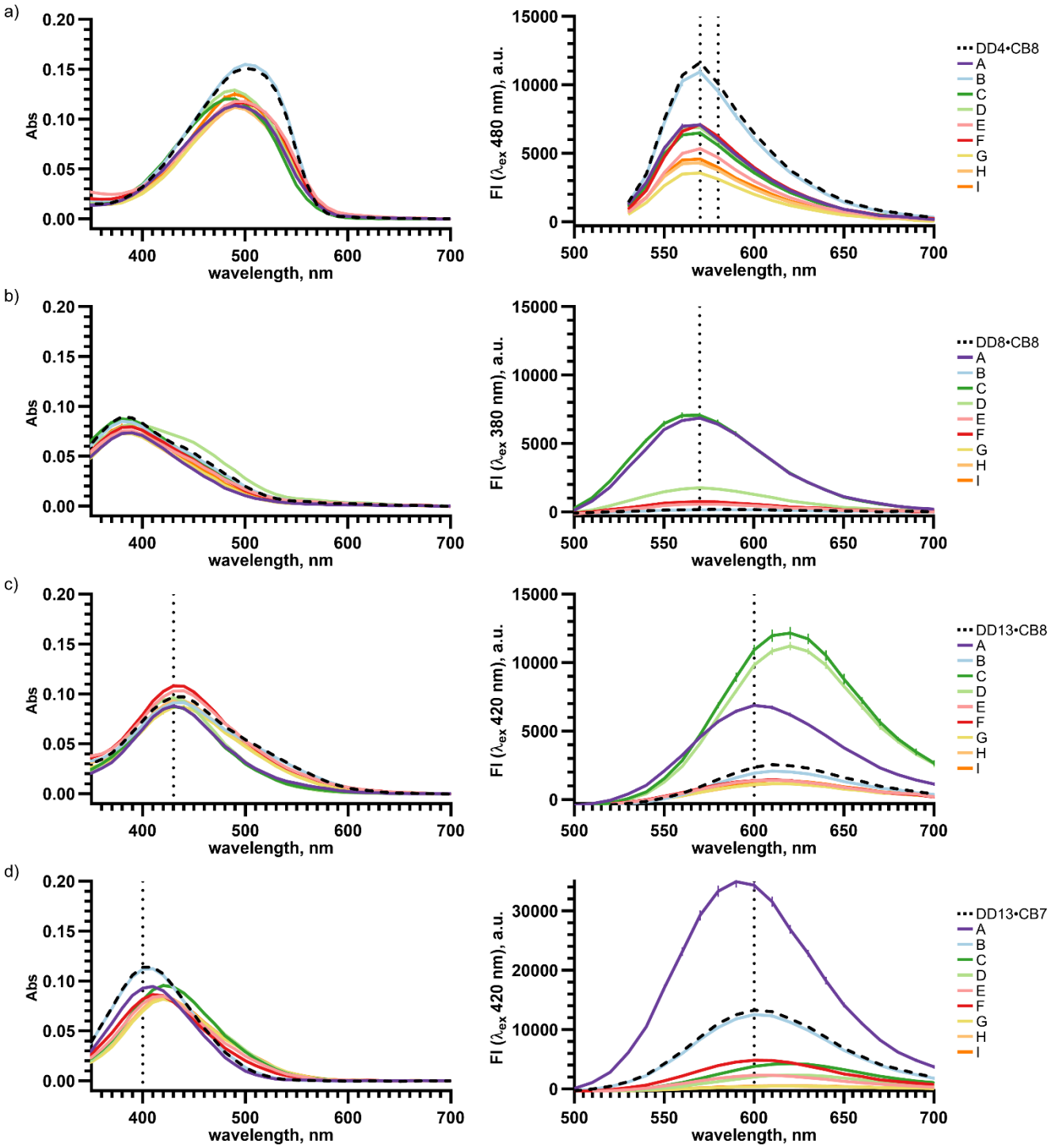

Figure S25. Mixed host chemosensor absorbance and fluorescence responses to multi-component street drug samples. Absorbance responses (left) and fluorescence responses (right) of mixed host chemosensors a) DD4•CB8, b) DD8•CB8, c) DD13•CB8 and d) DD13•CB7 to multi-component street drug samples A-I (Table 1, Figure S18). The dotted lines in the spectra represent the selected wavelengths used in PCA analysis (Table S3). Samples contain [DD] = 10.5 μM, [CB] = 21 μM, and [street drug sample] = 0.03 mg/mL. All samples are in NaH_2PO_4/Na_2HPO_4 (8.4 mM, pH 7.4) in H_2O with 2% MeOH.

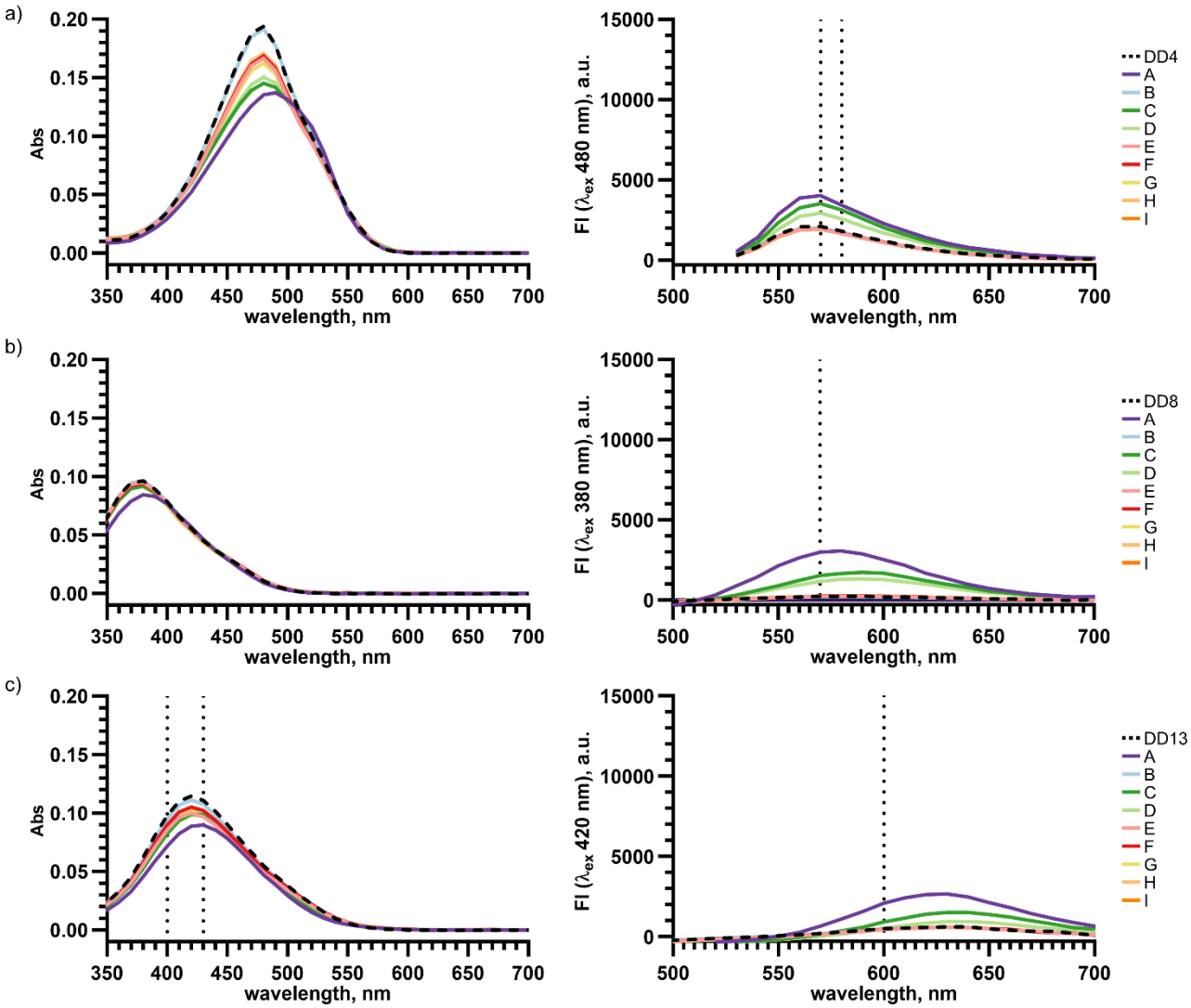

Figure S26. DimerDye absorbance and fluorescence responses to multi-component street drug samples. Absorbance responses (left) and fluorescence responses (right) of DimerDyes a) DD4 b) DD8 and c) DD13 to multi-component street drug samples A-I (Table 1, Figure S18). The dotted lines in the spectra represent the selected wavelengths used in PCA analysis (Table S4). Samples contain [DD] = 10.5 µM and [street drug sample] = 0.03 mg/mL. All samples are in NaH_2PO_4/Na_2HPO_4 (8.4 mM, pH 7.4) in H_2O with 2% MeOH.

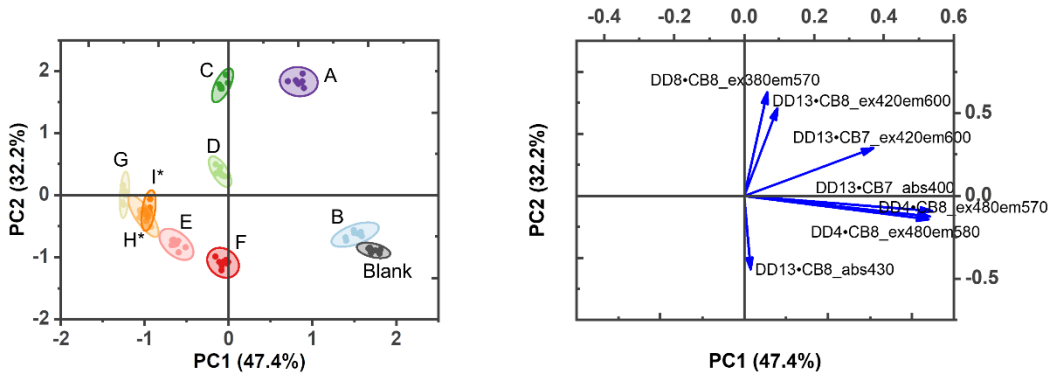

Figure S27. An array of mixed host chemosensors differentiates multi-component street drug samples. Sensor array includes absorbance and fluorescence responses from mixed host chemosensors DD4•CB8, DD8•CB8, DD13•CB8, and DD13•CB7. PCA (correlation) score plot shows each sample set (n = 8) enclosed by 95% confidence ellipses the respective loading plot of absorbance and fluorescence variables shown as blue vectors. Samples contain [DD] = 10.5 µM, [CB] = 21 µM, and [street drug sample] = 0.03 mg/mL. All samples are in NaH_2PO_4/Na_2HPO_4 (8.4 mM, pH 7.4) in H_2O with 2% MeOH.

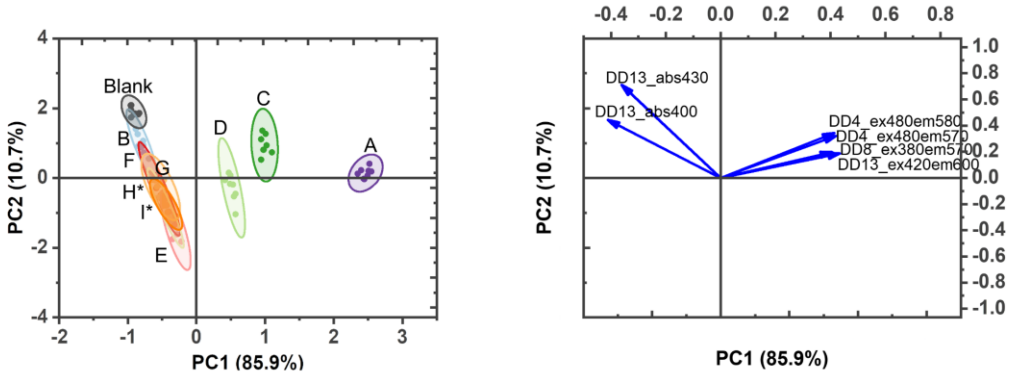

Figure S28. An array of DimerDye chemosensors does not differentiate street drug samples. PCA (correlation) score plot shows each samples set (n = 8) enclosed by 95% confidence ellipses with the respective loading plot of absorbance and fluorescence variables shown as blue vectors. Samples contain [DD] = 10.5 µM and [street drug sample] = 0.03 mg/mL. All samples are in NaH_2PO_4/Na_2HPO_4 (8.4 mM, pH 7.4) in H_2O with 2% MeOH.

References

1. M. A. Beatty, A. J. Selinger, Y. Li and F. Hof, Parallel Synthesis and Screening of Supramolecular Chemosensors that Achieve Fluorescent Turn-on Detection of Drugs in Saliva, *J. Am. Chem. Soc.* , 2019, **141**, 16763-16771.
2. J. Kim, I.-S. Jung, S.-Y. Kim, E. Lee, J.-K. Kang, S. Sakamoto, K. Yamaguchi and K. Kim, New Cucurbituril Homologues: Syntheses, Isolation, Characterization, and X-ray Crystal Structures of Cucurbit[*n*]uril (n = 5, 7, and 8), *J. Am. Chem. Soc.*, 2000, **122**, 540-541.
3. D. Jiao and O. A. Scherman, Isolation of cucurbit[n]uril homologues with imidazolium salts in a recyclable manner, *Green Chem.* , 2012, **14**, 2445.
4. A. J. Blacker, J. Jazwinski and J.-M. Lehn, Molecular Anion Binding and Substrate Photooxidation in Visible Light by 2,7-Diazapyrenium Cations, *Helv. Chim. Acta.*, 1987, **70**, 1-12.
5. Substance: Vancouver Island Drug Checking Project, https://substance.uvic.ca.
6. B. Wallace, R. Hills, J. Rothwell, D. Kumar, I. Garber, T. Van Roode, A. Larnder, F. Pagan, J. Aasen, J. Weatherston, L. Gozdzialski, M. Ramsay, P. Burek, M. S. Azam, B. Pauly, M. A. Storey and D. Hore, Implementing an integrated multi-technology platform for drug checking: Social, scientific, and technological considerations, *Drug Test Anal.* , 2021, **13**, 734-746.
7. L. Gozdzialski, A. Hutchison, B. Wallace, C. Gill and D. Hore, Toward Automated Infrared Spectral Analysis in Community Drug Checking, *Drug Test Anal.* , 2023, DOI: 10.1002/dta.3520.
8. S. A. Borden, A. Saatchi, G. W. Vandergrift, J. Palaty, M. Lysyshyn and C. G. Gill, A New Quantitative Drug Checking Technology for Harm Reduction: Pilot Study in Vancouver, Canada Using Paper Spray Mass Spectrometry, *Drug Alcohol Rev.*, 2022, **41**, 410-418.
9. S. A. Borden, A. Saatchi, E. T. Krogh and C. G. Gill, Rapid and Quantitative Determination of Fentanyls and Pharmaceuticals from Powdered Drug Samples by Paper Spray Mass Spectrometry, *Anal. Sci. Adv.* , 2020, **1**, 97-108.
10. L. Gozdzialski, A. Rowley, S. A. Borden, A. Saatchi, C. G. Gill, B. Wallace and D. K. Hore, Rapid and Accurate Etizolam Detection Using Surface-Enhanced Raman Spectroscopy for Community Drug Checking, *Int. J. Drug Policy*, 2022, **102**, 103611.
11. Paper Spray Mass Spectrometry Target List by Category, https://substance.uvic.ca/paperspray.
12. A. Krezel and W. Bal, A Formula for Correlating pK_a Values Determined in D_2O and H_2O, *J. Inorg. Biochem.* , 2004, **98**, 161-166.
13. A. Prabodh, D. Bauer, S. Kubik, P. Rebmann, F. G. Klärner, T. Schrader, L. Delarue Bizzini, M. Mayor and F. Biedermann, Chirality Sensing of Terpenes, Steroids, Amino Acids, Peptides and Drugs with Acyclic Cucurbit[*n*]urils and Molecular Tweezers, *Chem. Commun.*, 2020, **56**, 4652-4655.
14. A. Prabodh, S. Sinn and F. Biedermann, Analyte Sensing with Unselectively Binding Synthetic Receptors: Virtues of Time-Resolved Supramolecular Assays, *Chem. Commun.*, 2022, **58**, 13947-13950.
15. D. F. Swinehart, The Beer-Lambert Law, *J. Chem. Educ.*, 1962, **39**, 333.
16. M. A. Beatty, J. Borges-González, N. J. Sinclair, A. T. Pye and F. Hof, Analyte-Driven Disassembly and Turn-On Fluorescent Sensing in Competitive Biological Media, *J. Am. Chem. Soc.* , 2018, **140**, 3500-3504.
17. C. Gallo, S. S. Thomas, A. J. Selinger, F. Hof and C. Bohne, Mechanism of a Disassembly-Driven Sensing System Studied by Stopped-Flow Kinetics, *J. Org. Chem.*, 2021, **86**, 10782-10787.
18. J. Liu, H. Lambert, Y.-W. Zhang and T.-C. Lee, Rapid Estimation of Binding Constants for Cucurbit[8]uril Ternary Complexes Using Electrochemistry, *Anal. Chem.*, 2021, **93**, 4223-4230.
19. F. Biedermann, I. Ross and O. A. Scherman, Host–guest accelerated photodimerisation of anthracene-labeled macromolecules in water, *Polym. Chem.*, 2014, **5**.
20. M. Sayed, F. Biedermann, V. D. Uzunova, K. I. Assaf, A. C. Bhasikuttan, H. Pal, W. M. Nau and J. Mohanty, Triple emission from p-dimethylaminobenzonitrile-cucurbit[8]uril triggers the elusive excimer emission, *Chem. Eur. J.* , 2015, **21**, 691-696.
21. S. Zhang, L. Grimm, Z. Miskolczy, L. Biczók, F. Biedermann and W. M. Nau, Binding affinities of cucurbit[*n*]urils with cations, *Chem. Commun.*, 2019, **55**, 14131-14134.
22. A. Shrivastava, Methods for the determination of limit of detection and limit of quantitation of the analytical methods, *Chron. Young Sci.*, 2011, **2**, 21-25.
23. S. Stewart, M. A. Ivy and E. V. Anslyn, The use of principal component analysis and discriminant analysis in differential sensing routines, *Chem. Soc. Rev.*, 2014, **43**, 70-84.